

**1 Bifurcation points for tropical cyclone genesis and intensification in sheared
2 and dry environments**

3 Chaehyeon C. Nam,^a Michael M. Bell,^a and Dandan Tao^{a,b}

4 ^a Colorado State University, Fort Collins, Colorado

5 ^b University of Bergen, Bergen, Norway

6 Corresponding author: Chaehyeon Chelsea Nam, c.chelsea.nam@colostate.edu

7 ABSTRACT: The combination of moderate vertical wind shear (VWS) and dry environments
8 can produce the most uncertain scenarios for tropical cyclone (TC) genesis and intensification. We
9 investigated the sources of increased uncertainty of TC development under moderate VWS and
10 dry environments using a set of Weather Research and Forecasting (WRF) ensemble simulations.
11 Statistical analysis of ensemble members for precursor events and time-lagged correlations indicates
12 that successful TC development is dependent on a specific set of precursor events. A deficiency
13 in any of these precursor events leads to a failure of TC intensification. The uncertainty of TC
14 intensification can be largely attributed to the probabilistic characteristics of precursor events
15 lining up together before TC intensification. The critical bifurcation point between successful and
16 failed trials in these idealized simulations is the sustained vortex alignment process. Even for the
17 failed intensification cases, most simulations showed deep organized convection, which reformed
18 a mid-level vortex. However, for the failed cycles, the new mid-level vortex could not sustain
19 vertical alignment with the low-level center and was carried away by VWS shortly. Under the
20 most uncertain setup (VWS 7.5 m s^{-1} and 50% moisture), the latest developing ensemble member
21 had seven events of tilt decreasing and increasing again that occurred during the eight days before
22 genesis. Some unsuccessful precursor events looked very close to the successful ones, implying
23 limits on the intrinsic predictability for TC genesis and intensification in moderately sheared and
24 dry environments.

25 SIGNIFICANCE STATEMENT: The aim of this study is to identify a critical bifurcation point
26 that determines whether tropical disturbances in moderately sheared and dry environments will
27 develop into intense storms or dissipate. When it comes to predicting the formation and strength of
28 tropical cyclones, vertical wind shear, where the environmental wind changes with height, presents
29 a challenging scenario. When the shear is neither too weak nor too strong, some systems manage to
30 develop into cyclones, while others get torn apart under similar shear conditions. Understanding the
31 differences between these outcomes remains a puzzle. Through extensive computer simulations,
32 we have discovered a key factor that contributes to the uncertainty surrounding the alignment of the
33 mid-level vortex with the center of the low-level vortex. These results reveal the complexity and
34 multiple sources of uncertainty involved in forecasting tropical cyclone intensification, providing
35 valuable insights into why moderate shear is a particularly challenging regime to predict tropical
36 genesis and intensification.

37 1. Introduction

38 Vertical wind shear (VWS) is one of the most important factors for TC genesis and intensity
39 change. Weak VWS provides a favorable environment for TC development, while strong VWS
40 could disintegrate the TC vortex (e.g., Bracken and Bosart 2000; Nolan and McGauley 2012).
41 Moderate vertical wind shear (VWS) is defined as the range of VWS magnitudes that are neither
42 too weak to have negligible impacts on TC intensity change nor too strong to completely thwart
43 TC intensification with the range of $4.5 - 11 \text{ m s}^{-1}$ (Rios-Berrios and Torn 2017). Both ensemble
44 modeling studies and analyses of operational intensity forecast errors have shown that tropical
45 cyclogenesis and intensification are the most unpredictable with moderate VWS (Zhang and Tao
46 2013; Finocchio and Majumdar 2017; Bhatia and Nolan 2013). The climatological study of Rios-
47 Berrios and Torn (2017) also verified that the likelihood of intensifying or weakening is comparable
48 with moderate VWS, whereas the likelihood is skewed toward intensification or weakening for weak
49 and strong VWS, respectively.

50 Another factor that increases uncertainty around tropical cyclogenesis is environmental dry
51 air. Moisture is essential to sustain diabatic convection and the associated vorticity generation and
52 secondary circulation that intensify tropical cyclones, such that a drier atmosphere can suppress TC
53 development. Studies comparing developing and nondeveloping tropical disturbances have found

that a key difference between the two groups is the moisture, especially the mid-level humidity (Peng et al. 2012; Montgomery et al. 2012; Davis and Ahijevych 2013). The dry mid-level air affects the overall upward vertical mass flux via entrainment of less buoyant air parcels (i.e., radial ventilation; James and Markowski 2010) and convective downdrafts into the subcloud layer (i.e., downward ventilation), which result in a longer recovery time for subsequent deep convection (Riemer et al. 2010; Alland et al. 2017). The combination of dry air and moderate VWS can further increase the uncertainties leading to TC genesis and intensification as alluded by Tang and Emanuel (2012) and Tao and Zhang (2014), with dynamic processes interacting with the thermodynamic processes of moistening (Tang et al. 2020). For example, the ventilation process is more efficient when the vortex tower is tilted by VWS as both radial and downward ventilation can more easily impact the inner-core convection (Alland et al. 2021a,b).

In this study, we aim to gain a process-based understanding of why the combination of moderate VWS and environmental dry air makes an uncertain setup for the early phase of TC development. A developing TC is at the border of two scales, the quasi-balanced synoptic scale and the stochastic cloud-organizing mesoscale (Ooyama 1982). Our hypothesis is that the stochastic character of diabatic convection becomes more important for TC genesis and intensification in marginally favorable environments such as moderately sheared and dry environments.

Recent observational and modeling studies have revealed that TCs that successfully develop or intensify under moderate to large VWS undergo vortex restructuring processes such as "downshear reformation" (Nguyen and Molinari 2015; Rios-Berrios et al. 2018; Chen et al. 2018; Nam and Bell 2021). The downshear reformation process starts with convection shifted to the downshear area by the VWS. Inside the convective area in the downshear region, the vertical component of vorticity is produced through tilting of horizontal vorticity, vortex stretching, and vertical advection of vorticity. The newly produced vorticity is accumulated inside the broader circulation through a vortex merger process. Thus, multiple thermodynamic and dynamic processes need to come together: namely, deep convection in the downshear region, vorticity generation, and vortex alignment through vortex merger. Then, our question is which processes may lead to bifurcation points between the TCs that do develop and the ones that do not intensify under the same magnitude of VWS.

Nine sets of idealized TC simulations with 20-member ensembles with varying VWS magnitude and environmental humidity are used to answer the above scientific question. Ensemble numerical

84 simulations have been widely used by previous studies as means to investigate the intrinsic pre-
85 dictability of weather and TCs (e.g., Lorenz 1969; Melhauser and Zhang 2012). We investigated
86 the TC characteristics leading to TC intensification: vertical realignment of the vortex tower,
87 organized deep convection near the vortex center, and vortex strength (e.g., Wang 2012; Tao and
88 Zhang 2014, 2015; Alland et al. 2021a). The rest of this paper is outlined as follows. Section 2
89 outlines the experimental design and the ensemble model setup. Section 3 describes the results
90 from those simulations. Section 4 synthesizes the results and explores the underlying cause of
91 the uncertainties for the marginally favorable environments, and discusses the implications of our
92 findings from the idealized simulations for real TCs.

93 **2. Experiment Setup**

94 Tropical cyclone interactions with VWS and a dry environment were simulated in this study with
95 the Advanced Research version of Weather Research and Forecasting (ARW-WRF; Skamarock
96 et al. 2008) Model (version 3.1.1). We note that the simulations analyzed in this paper were
97 previously shown and analyzed from an ensemble mean perspective in Tao and Zhang (2014). We
98 ran sensitivity tests with a newer version of WRF (3.9) and found that the initial vortices spin up
99 earlier in WRF 3.9 compared to WRF 3.1.1 but the main mechanisms that we identify did not
100 change (not shown, see Nam (2021) for details).

101 Three two-way nested domains were used with 18-, 6-, and 2-km horizontal grid spacing. The
102 three domains contained 240 x 240, 240 x 240, and 360 x 360 grid points, respectively, which
103 yields the domain sizes of 4320 km x 4320 km, 1440 km x 1440 km, and 720 km x 720 km. All
104 domains had 40 vertical levels, with the model top at 20 km. The two inner domains were designed
105 to follow the center of the vortex center at 850 hPa level. The configuration and choice of physics
106 packages included Yonsei University (YSU) boundary layer scheme (Hong et al. 2006), WRF
107 single-moment 6-class (WSM6) microphysics (Hong et al. 2004). No cumulus parameterization
108 nor short- or long-wave radiation schemes were used in our simulations. Not including radiation
109 could delay TC development (Rios-Berrios 2020) and exclude the impacts from diurnal pulses of
110 convection (Dunion et al. 2014). We discuss sensitivities to radiation more in Section 4.

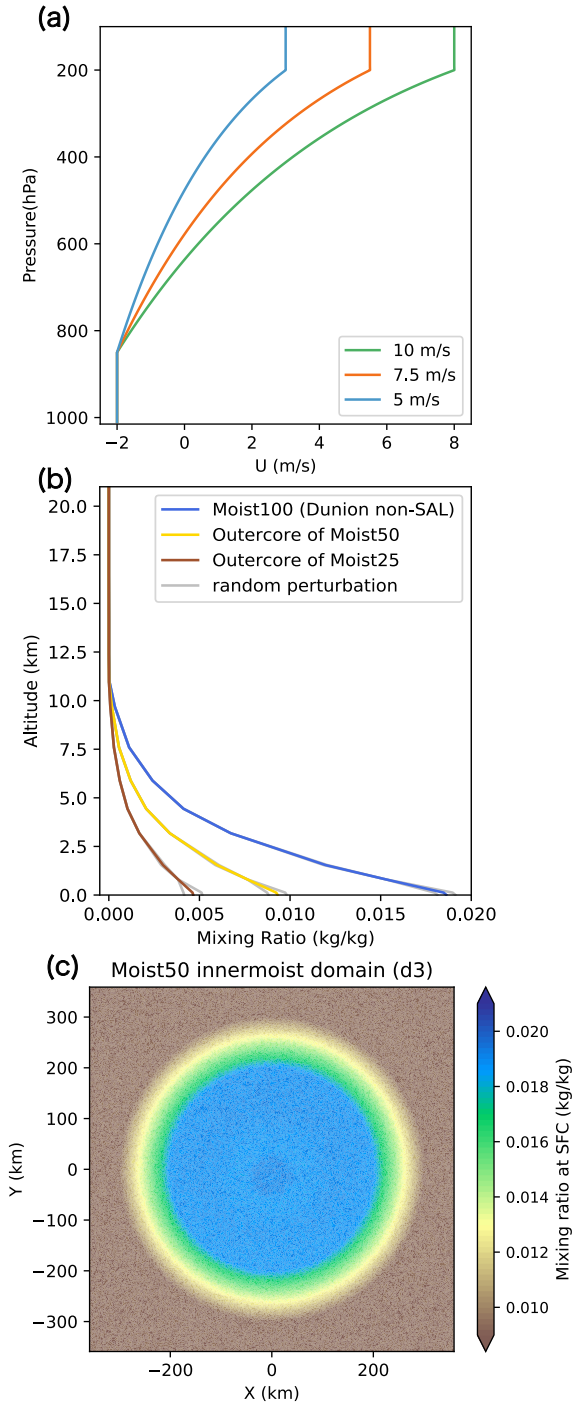
111 For all simulations, a weak, warm-core vortex was prescribed in the initial conditions with a
112 modified Rankine vortex profile having a set maximum tangential wind of 15 m s^{-1} at 850 hPa

height and 135-km radius. Tangential winds vanish at an 800-km radius and decay vertically following an exponential function (Moon and Nolan 2010). All simulations were set on a constant sea surface temperature (SST) of 29 °C and a constant planetary vorticity (i.e., a doubly periodic f-plane) corresponding to 20°N.

Around the tropical cyclone-like vortex, different profiles of environmental winds and thermodynamic soundings were specified. Figure 1 describes the environmental setup. Figure 1a shows the vertical profile of zonal winds that is prescribed for the simulations. For SH5, SH7.5, and SH10 configurations, westerly vertical wind shear (200 - 850 hPa) of 5, 7.5, and 10 m s⁻¹ was imposed with a method of “point-downscaling” developed by Nolan (2011). We note that the point-downscaling method forces VWS without imposing the temperature gradient induced by the shear and according to the thermal wind balance equation. With 10 m s⁻¹ VWS and 720 km domain size, the maximum temperature difference is around 1°C, which is not negligible but still quite small (see Appendix A of Tao (2015) for details).

For Moist100 simulations, the Dunion and Marron (2008) non-SAL mean hurricane season sounding was used for the initial thermodynamic profile following Zhang and Tao (2013). The Dunion and Marron (2008) non-SAL mean sounding (calculated from 2002) is moister in the lower levels compared to the moist tropical sounding in Dunion (2011) (calculated from 1995-2002). To investigate the impact of environmental dry air, the initial field of water vapor mixing ratio was modified as shown in Fig. 1b, as the water vapor mixing ratio for all heights in outer-core regions (outside the radius of 300 km) is reduced to 50% and 25% of the Dunion non-SAL sounding for Moist50 and Moist25 sets. For all simulations, the moisture is the same in the inner-core regions (within a 200 km radius), and between 200- and 300-km radius, the moisture decreased linearly (see Fig. 1c). Throughout the simulation hours, both the wind and water vapor fields are allowed to evolve from their initial values.

Each set of experiments consists of 20 ensemble members. The size of 20 ensemble members may not be enough to capture the full range of the possible outcomes, but our goal is not ensemble prediction of real TCs that should aim for the true spread. In this study, we aim to understand the physical factors that lead to increased uncertainty in TC genesis and intensification in marginally favorable environments. For that purpose, we chose 20 members consistent with previous idealized TC modeling studies (e.g., Rios-Berrios 2020; Tao and Zhang 2015). To



126 Fig. 1. Vertical profiles of **(a)** environmental zonal wind for SH5, SH7.5 and SH10 experiments **(b)** water
 127 vapor mixing ratio for the outer-core region (≥ 300 km radius) for Moist100, Moist50, Moist 25; **(c)** Water vapor
 128 mixing ratio at the surface level from one of the Moist50 experiments.

146 generate the ensembles, small amplitude random moisture perturbations are introduced; the initial
147 field of water vapor mixing ratio below 950 hPa was perturbed with random noise between -0.5 –
148 0.5 g kg⁻¹ sampled from a uniform distribution (Zhang and Tao 2013; Judt et al. 2016). We have
149 conducted sensitivity tests with more realistic dry soundings of Saharan Air Layer (SAL) (Dunion
150 2011) and mid-level dry intrusion (Martinez et al. 2020) and the SAL runs were similar to the
151 Moist50 set (not shown). More discussion about the sensitivity tests can be found in Section 4.

152 With the three different shear profiles and three moisture profiles, there are, in total, nine
153 different experimental sets to investigate the combined impacts of shear and dry air. Table 1 shows
154 descriptions of all the ensemble sets analyzed in this study.

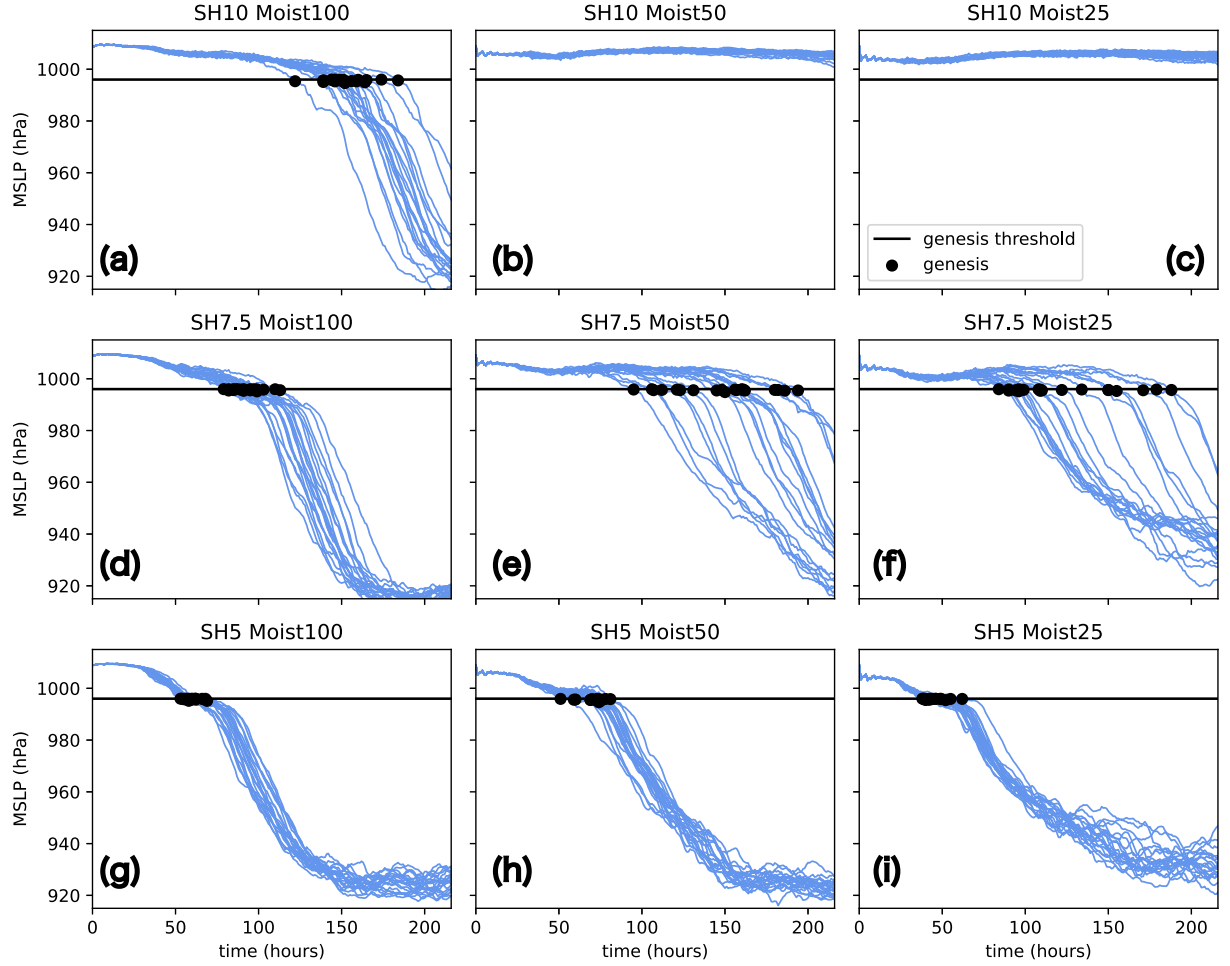
TABLE 1. List of experiments with corresponding experimental setups.

| Set Name | Wind Shear | Outer-core Moisture |
|----------------|-----------------------|---------------------|
| SH10_Moist100 | 10 m s ⁻¹ | Dunion Non-SAL |
| SH10_Moist50 | 10 m s ⁻¹ | 50% of Moist100 |
| SH10_Moist25 | 10 m s ⁻¹ | 25% of Moist100 |
| SH7.5_Moist100 | 7.5 m s ⁻¹ | Dunion Non-SAL |
| SH7.5_Moist50 | 7.5 m s ⁻¹ | 50% of Moist100 |
| SH7.5_Moist25 | 7.5 m s ⁻¹ | 25% of Moist100 |
| SH5_Moist100 | 5 m s ⁻¹ | Dunion Non-SAL |
| SH5_Moist50 | 5 m s ⁻¹ | 50% of Moist100 |
| SH5_Moist25 | 5 m s ⁻¹ | 25% of Moist100 |

155 3. Results

156 a. Overview of TC development

160 In our study, the timing of TC genesis is determined as the timing of the simulation obtaining
161 MSLP below a threshold of 996 hPa as the onset of sustained intensification. It can be challenging
162 to determine the exact timing of TC genesis for a simulated tropical disturbance. Tang et al. (2020)
163 described TC genesis, based on WMO (2017), as “the development from a tropical disturbance
164 – a discrete tropical (or subtropical) weather system of apparently organized convection – to a
165 tropical depression (TD) or tropical storm (TS) – a warm-core, non-frontal, synoptic-scale cyclone
166 with organized deep convection and a closed surface wind circulation about a well-defined center”.
167 This somewhat subjective definition highlights the lack of quantitative guidelines to identify TC



157 FIG. 2. Time series of hourly minimum sea level pressure for 20 ensemble members of nine experimental
 158 sets. Timings of tropical cyclogenesis are marked with black circles. Each time series is smoothed using a 12-hr
 159 low-pass Lanczos filter with nine weights.

168 genesis. In the continuum of states of tropical intensity, we decided to use TS designation (when
 169 the TC is named if it were a real storm) to define the genesis time for each simulated TC similar to
 170 previous TC genesis studies (Bell and Montgomery 2019; Murthy and Boos 2018). The guidance
 171 of Dvorak CI-number of 2.5, which corresponds to the transition from TD to weak TS, correlates
 172 with 13 hPa deficit of central pressure (ΔP) (Knaff and Zehr 2007; Courtney and Knaff 2009).
 173 In our idealized simulations, the environmental SLP (the initial SLP of the outermost domain far
 174 enough from the initial vortex) was uniform around 1009 hPa, so 996 hPa corresponds to 13 hPa of
 175 ΔP compared to the environments. We decided to use MSLP rather than maximum wind speed to

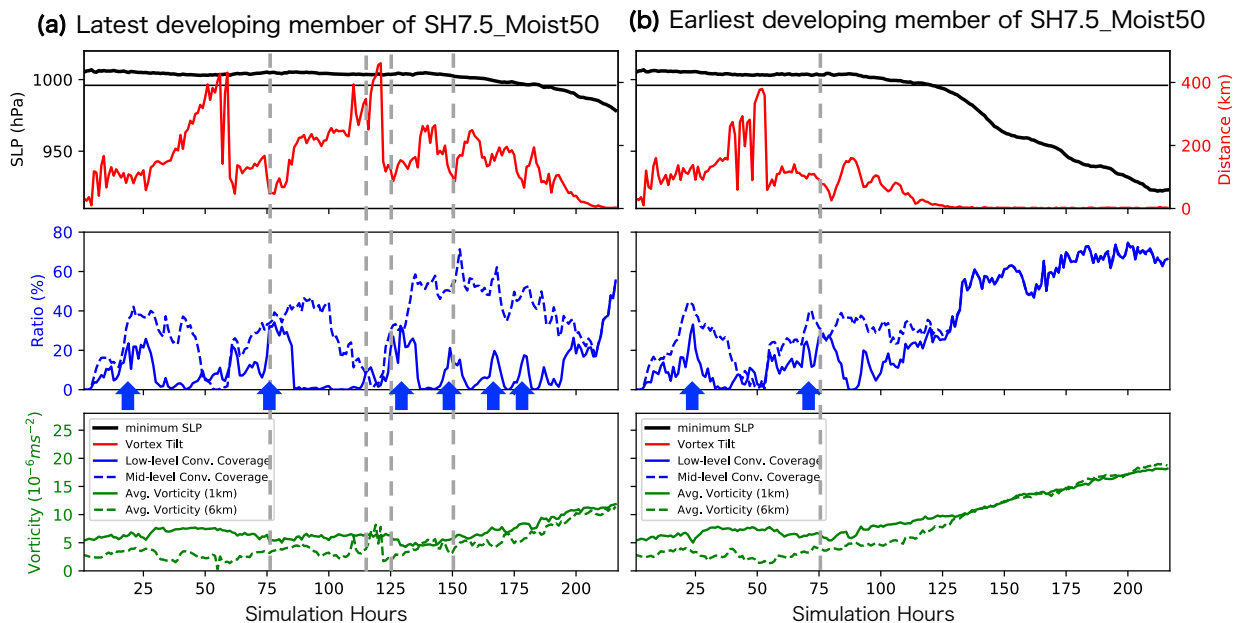
measure TC genesis and intensification because the central pressure deficit is an intensity measure that combines maximum wind speed, storm size, and background rotation rate (Chavas et al. 2017), and is easier to estimate and more stable with time than maximum wind speed (Klotzbach et al. 2020).

Vertical wind shear (VWS) and dry air together have profound impacts on the evolution of simulated tropical cyclones. Fig. 2 displays the time series of minimum sea level pressure (MSLP) for the nine ensemble sets. For all ensembles, the simulated tropical cyclones undergo only minimal MSLP deepening during the first 36 hours. Substantial differences depending on VWS and environmental humidity appear after the first 36 hours. In general, the weaker VWS and the more moisture, the earlier ensembles develop. The average timing of genesis for the three SH5 sets is similar (see Fig. 2 g, h, i). Most of the SH5 ensembles reach a steady state of MSLP around 150 hours and the steady-state MSLP is lower in the moister simulations through the simulation time (Figs. 2 g, h, i). For the strongest VWS of 10 m s^{-1} , only the ensembles with Moist100 underwent genesis during the nine days of simulation time, and no ensembles from SH10_Moist50 and SH10_Moist25 reached a point of tropical cyclogenesis (Fig. 2 a, b, c). SH7.5_Moist100 is right in between SH5_Moist100 and SH10_Moist100 in terms of genesis timing and ensemble spread (Fig. 2d).

The largest ensemble spread was found in the drier sets of SH7.5 (Fig. 2 e,f). The standard deviation of MSLP from 20 ensemble members of SH7.5_Moist50 was 18.8 hPa at median genesis time (153 hour) and reached a maximum of 23.2 hPa at 191 hour. The second largest ensemble spread was found from SH7.5_Moist25 with a maximum of 21.7 hPa at 166 hour. For SH10, the dry environment simply eliminated the possibility of TC development, and for SH5, the ensemble spread was still pretty narrow (maximum 6.3 and 6.2 hPa for SH5_Moist50 and SH5_Moist25), not so different from Moist100 simulations (maximum 7.0 hPa). In contrast, for SH7.5, having a drier environment made the ensemble spread of the MSLP time series much larger, which implies a difficult forecast problem; minimal amounts of random water vapor perturbation produced completely different TC development scenarios with 99 hours difference in genesis timing between the earliest developing member and the latest developing member of SH7.5_Moist50.

204 *b. Bifurcation points for TC intensification for SH7.5_Moist50*

205 We looked into each ensemble member under the experiment that showed the widest ensemble
 206 spread, the moderately sheared and dry environment of SH7.5_Moist50, to investigate how the
 207 minimal random perturbations could produce such a wide gap in the timing of TC genesis. In
 208 Fig. 3, we contrast the latest and the earliest developing members of SH7.5_Moist50 set similar
 209 to Rios-Berrios et al. (2016) who analyzed TC intensification of Ophelia (2011) comparing strong
 210 and weak ensemble members. In addition to MSLP, the time series of vortex tilt, inner-core
 211 convective coverage (low-level and mid-level), and average vorticity (low-level and mid-level) are
 212 shown. Here, low-level refers to 1 km altitude, and mid-level refers to 6 km altitude.



213 FIG. 3. Time series of variables show thermodynamic and dynamic processes leading to intensification
 214 for (a) latest developing ensemble member and (b) earliest developing ensemble member of SH7.5_Moist50
 215 experimental set. Blue arrows mark distinctive low-level convective bursts. Grey dashed lines indicate the
 216 timesteps (Hour-75, Hour-115, Hour-125, Hour-150) highlighted in Figs. 5 – 8 for latest member and the
 217 timestep of Hour-75 in Fig. 4 for the earliest member.

218 It is necessary to explain how we calculated these variables to lay out what each variable
 219 represents. All variables were interpolated in the vertical coordinate from the WRF sigma levels to

220 altitude (from 0 km to 22 km in a 400 m interval) using the geopotential height and pressure outputs.
221 First, the vortex center at each vertical level is detected as the location of minimum pressure with
222 the pressure field smoothed with a Gaussian filter with sigma (the standard deviation for Gaussian
223 kernel) of 10 grid points. We confirmed that our findings hold when the vortex centers are
224 calculated using the pressure centroid method (Nguyen et al. 2014). Second, convective coverage
225 indicates the proportion of area inside the inner-core region (200 km x 200 km box around the
226 vortex center) that is covered by convection. We used 20 dBZ at a 6-km altitude as the threshold
227 to indicate a convective grid cell (Rogers et al. 2015). The low-level convective coverage indicates
228 the convective coverage of the 200 km x 200 km box around the vortex center at 1 km, and the
229 mid-level convective coverage is measured inside the 200 km x 200 km box around the vortex
230 center at 6 km (e.g., panel b, d of Figs. 5 – 8). Thus, the low-level and mid-level convective
231 coverage will be identical if the vortex tilt is zero as the two boxes overlap. Lastly, the average
232 vorticity is the arithmetic mean of the relative vertical vorticity inside the 200 km x 200 km domain
233 surrounding the vortex center at the respective altitudes of 1 and 6 km. When the vortex tilt is large
234 (> 260 km), the 200 km x 200 km mid-level box can be cut off at the edge of the inner domain, and
235 for this case, the mid-level metrics are calculated over the smaller rectangular box (see Fig. 6a, c)

236 Comparing the two panels of Fig. 3 through the first 90 hours, the two ensemble members exhibit
237 a similar evolution. The vortex tilt increased and rapidly decreased with changing convective
238 coverage. For the latest developing member, multiple cycles (six cycles when counting each
239 distinctive low-level convective burst [see blue arrows in Fig.3]) occurred before genesis, whereas
240 the earliest developing member reached tropical cyclogenesis after going through two cycles. Here,
241 one cycle of the precursor event is defined as the precursor variable reaching a certain threshold
242 and maintaining the magnitude for more than three hours before the precursor event terminates.
243 How we set the specific thresholds for different precursor variables will be described in Section 3c.

244 The first convective cycle spanned about 48 hours for both members. Initially, convective
245 coverage increased in the inner-core region in the first 36 hours. As the vortex tilt increased while
246 the mid-level vortex was shifted eastward by westerly VWS, there emerged a discrepancy between
247 low-level and mid-level convective coverage. Low-level convective coverage decreased from 20%
248 to zero as tilt increased, but mid-level convective coverage remained relatively constant at 35% for
249 a longer time.

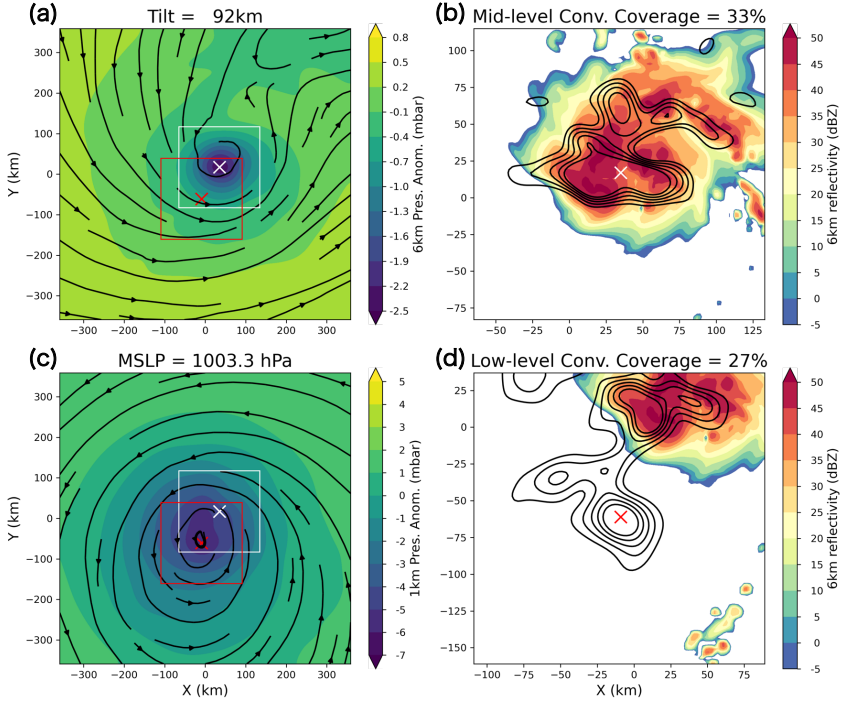
250 For both ensemble members, the second cycle started around 55 hours, with convective coverage
251 starting to increase again, and then around 60 hours, vortex tilt drastically decreased from 400
252 km to below 50 km. With the mid-level vortex being displaced 400 km from the low-level vortex
253 center, it is probably more accurate to consider these two distinct vortices rather than a vertically
254 coherent tilted vortex. Similar to the first cycle, as tilt increased again, low-level convective
255 coverage decreased around 85 hours. The bifurcation point between these two members appears
256 to be around 90 hours: the latest member's tilt kept increasing but the earliest member's tilt started
257 to diminish again. As tilt approached zero (mid-level and low-level vortices perfectly aligned), the
258 earliest developing member quickly passed the genesis phase and entered the rapid intensification
259 phase. The latest developing member took more cycles of tilt decreasing and multiple low-level
260 convective coverage bursts until it underwent genesis.

261 The average low- and mid-level vorticity steadily increase in concert with the steadily decreasing
262 trend of MSLP for both the earliest and latest developing members. In Fig. 3b, the mid-level
263 vorticity starts from a lower magnitude compared to the low-level vorticity but increases faster
264 than the low-level vorticity; they reach a similar magnitude of vorticity in about 24 hours after the
265 low-level vorticity starts to increase.

266 We examined the hourly pressure and reflectivity fields of the two ensemble members to investi-
267 gate the detailed process behind the repeated cycles of precursor events. Figures 5, 6, 7, and 8 show
268 the snapshots of the simulated TC of the latest ensemble member of SH7.5_Moist50 at hour-75,
269 hour-115, hour-125, and hour-150, respectively (grey dashed lines in Fig. 3a). To compare with
270 Fig. 5, Fig. 4 shows the snapshot of the earliest ensemble member at the same simulation hour
271 75 and its 2nd cycle of convective bursts. The hour-75 and hour-150 time steps are peaks in the
272 low-level convective coverage of the 2nd and 4th cycles for the latest developing member. The
273 hour-115 and hour-125 mark the times before and after the drastic tilt decrease during the early
274 phase of the 3rd cycle of the low-level convective bursts.

275 Figure 4 displays the pressure deficit and reflectivity at both the low-level (1 km) and mid-level (6
276 km) for the earliest ensemble member at hour-75. As expected with the westerly VWS, a mid-level
277 vortex appears northeast of the low-level vortex center (white 'x' and red 'x', respectively in Fig.
278 4a,c). The tilt was relatively small (92 km), and a mesoscale convective system was situated at the
279 center of the mid-level vortex. The mid-level vorticity contours align with deep convection within

Hour-75 of the fastest SH7.5_RH50



266 FIG. 4. Snapshot of simulated TC from the earliest developing member of SH7.5_Moist50 at hour-75 (Fig.3b).
267 Pressure anomaly and the streamlines at an altitude of (a) 6 km, (c) 1 km, simulated reflectivity at 6km inside
268 200 km x 200 km box around the center of (b) mid-level vortex center (defined at 6 km), (d) low-level vortex
269 center (defined at 1 km). Relative vorticity at 6 km and 1 km is plotted in black contour in (b) and (d) from
270 $1 \times 10^{-5} s^{-1}$ to $3 \times 10^{-5} s^{-1}$ in the interval of $5 \times 10^{-6} s^{-1}$. Red and white 'x' indicate the low-level and mid-level
271 vortex centers, respectively. The 200 km x 200 km red and white boxes in (a), (c) are centered on the low- and
272 mid-level vortex centers. The white box is zoomed in as the domain of (b), and the red box corresponds to the
273 domain of (d).

288 the mesoscale convective system (Fig. 4b). In contrast, at the same hour-75, the latest ensemble
289 member has a local maximum of low-level convective coverage. Despite this difference, Figs. 4
290 and 5 share similar characteristics in terms of the downshear left location of the mid-level vortex
291 and the same 33 % of mid-level convective coverage. However, the earliest member has a broader
292 low-level convective coverage and stronger low-level vorticity. Notably, the tilt was 101 km for
293 the latest developing member. A mesoscale convective system was present at the center of the
294 mid-level vortex. The mid-level vorticity contours correspond with deep convection within the

Hour-75 of the slowest SH7.5_RH50

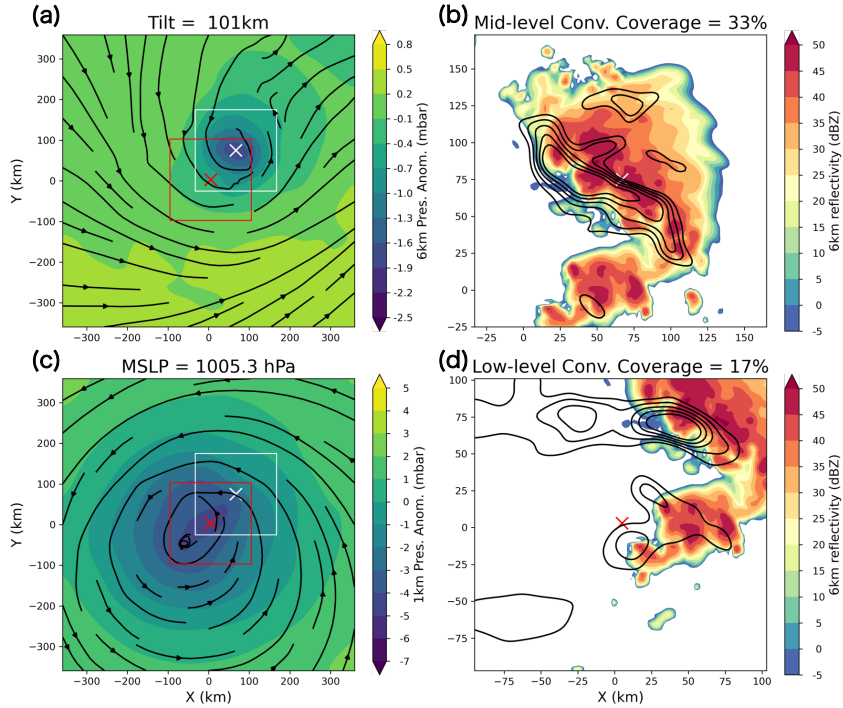


FIG. 5. Same as Fig. 4 but from the latest developing member at hour-75 (Fig.3 a)

Hour-115 of the slowest SH7.5_RH50

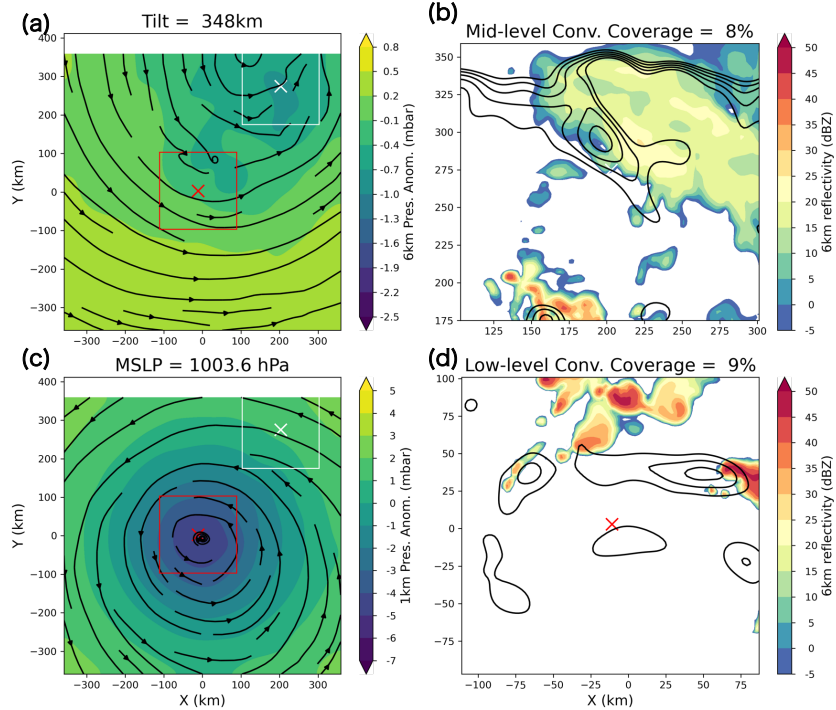


FIG. 6. Same as Fig. 4 but from the latest developing member at hour-115 (Fig.3 a)

Hour-125 of the slowest SH7.5_RH50

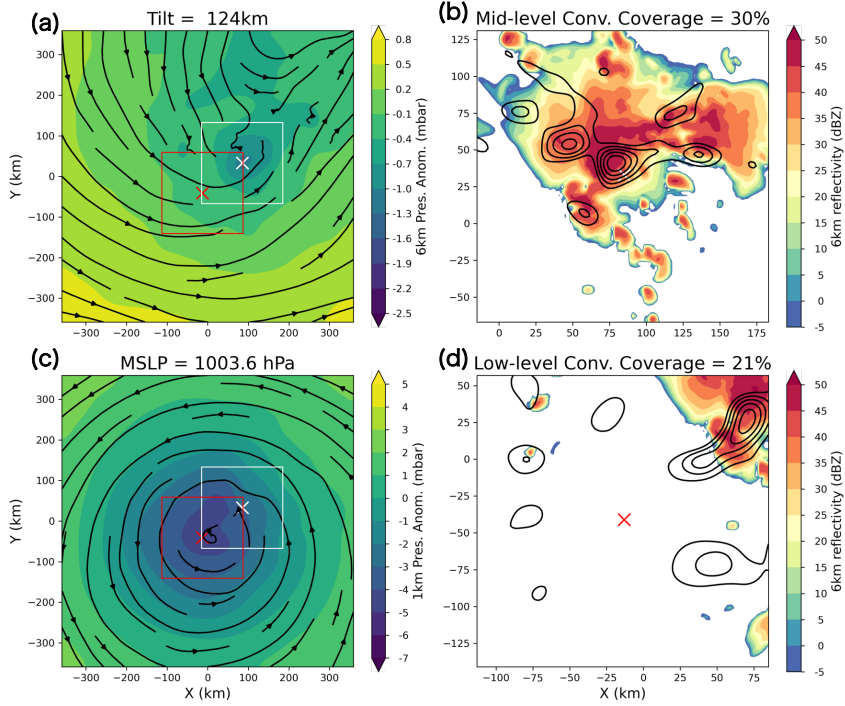


FIG. 7. Same as Fig. 4 but from the latest developing member at hour-125 (Fig.3 a)

Hour-150 of the slowest SH7.5_RH50

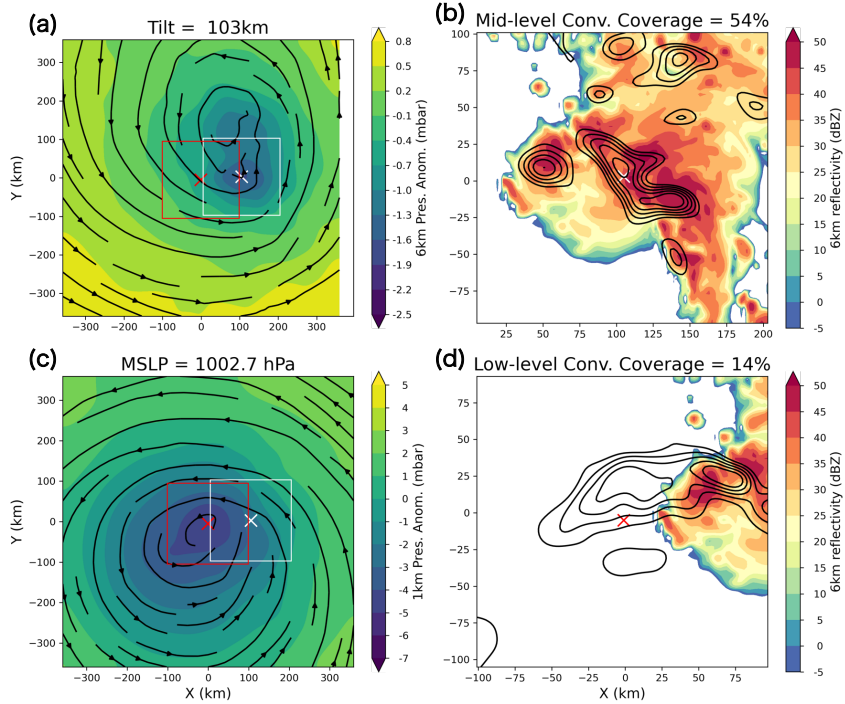


FIG. 8. Same as Fig. 4 but from the latest developing member at hour-150 (Fig.3 a)

mesoscale convective system (Fig. 5b). Taken together, Figs. 3, 4, and 5 suggest that at hour-75, it is challenging to predict which TC will develop in 36 hours and which will not develop for four days.

Figure 6 shows, for the latest developing member, that the mid-level vorticity shown in Fig. 5 was carried away northeastward by the westerly VWS. The 200 km x 200 km boxes centered around the mid-level and low-level vortex centers have much smaller convective coverage and vorticity not well aligned with convection. Ten hours later (in Fig. 7), the vortex tilt had decreased drastically because a new smaller mid-level vortex formed inside the deep mesoscale convective system. Looking at the hourly output of reflectivity, pressure, and vorticity fields at the mid-level (not shown), we confirmed that after the pre-existing mid-level vortex is advected away by the VWS, a new smaller scale (meso-beta scale) mid-level vortex forms at the same location of the deepest convection in downshear left quadrant, likely through vortex stretching by the deep convection. The idealized simulations of tilted TCs in Schecter and Menelaou (2020) also showed that tilt increase can be explained by adiabatic mechanisms, but tilt decrease can only be explained with the diabatic processes around the mesoscale convective systems.

From hour-125 to the time of TC genesis, the tilted vortex went through a prolonged vortex alignment process. Tilt kept fluctuating but never reached 400 km magnitude like before. From hour-125 (Fig. 7) to hour-150 (Fig. 8), the mid-level pressure deficit became larger, and the mid-level circulation became more robust, centered around the new mid-level vortex center. Mid-level convective coverage also grew larger.

A key question is why the newly formed mid-level vortex at the 2nd cycle (Fig. 5) did not result in TC intensification and was carried away, whereas the mid-level vortex at the 4th cycle (Fig. 8) persisted and resulted in intensification after the prolonged alignment process. Comparing Figs. 5 and 8, vortex tilt at these two times has similar magnitudes of 101 and 103 km, and the mid-level vortex is located northeast and east to the low-level vortex for hour-75 and hour-150. At both times, deep organized convection is located around the mid-level vortex center. One noticeable difference is that the mid-level vortex in hour-150 has a larger cyclonic circulation (see streamlines of Figs. 5a and 8a). While the increased size of the circulation may play a role, we have not done a detailed analysis of this factor. Further investigation into the specific characteristics that promote sustained vortex alignment is an important topic for future research.

325 The findings to highlight from Figs. 3 – 8 are:

- 326 • The earliest developing member and the latest developing member have similar behavior of
327 precursor events until the 90-hour mark.
- 328 • The latest developing member has multiple attempts at increasing convective coverage around
329 the low and mid-level vortex centers that could possibly lead to TC intensification. Still, they
330 all failed until the 6th attempt.
- 331 • Only after vortex tilt decreases closer to zero, SLP starts to drop rapidly.
- 332 • Low-level convective coverage is more episodic compared to mid-level convective coverage,
333 and mid-level convective coverage persists for a longer time after tilt increases again.
- 334 • Mid-level vorticity shows hints of increasing slightly sooner than low-level vorticity increasing
335 and SLP decreasing.
- 336 • Deep convection over a wider area inside the inner-core region generates a smaller-scale
337 mid-level vortex, which results in an instantaneous vortex tilt decrease.
- 338 • A key difference between the successful and failed precursor cycles in SH7.5_Moist50 ensem-
339 bles is whether the newly generated mid-level vortex sustains the alignment with the low-level
340 vortex or it is advected away by the VWS again.

341 *c. Probabilistic approach to TC intensification*

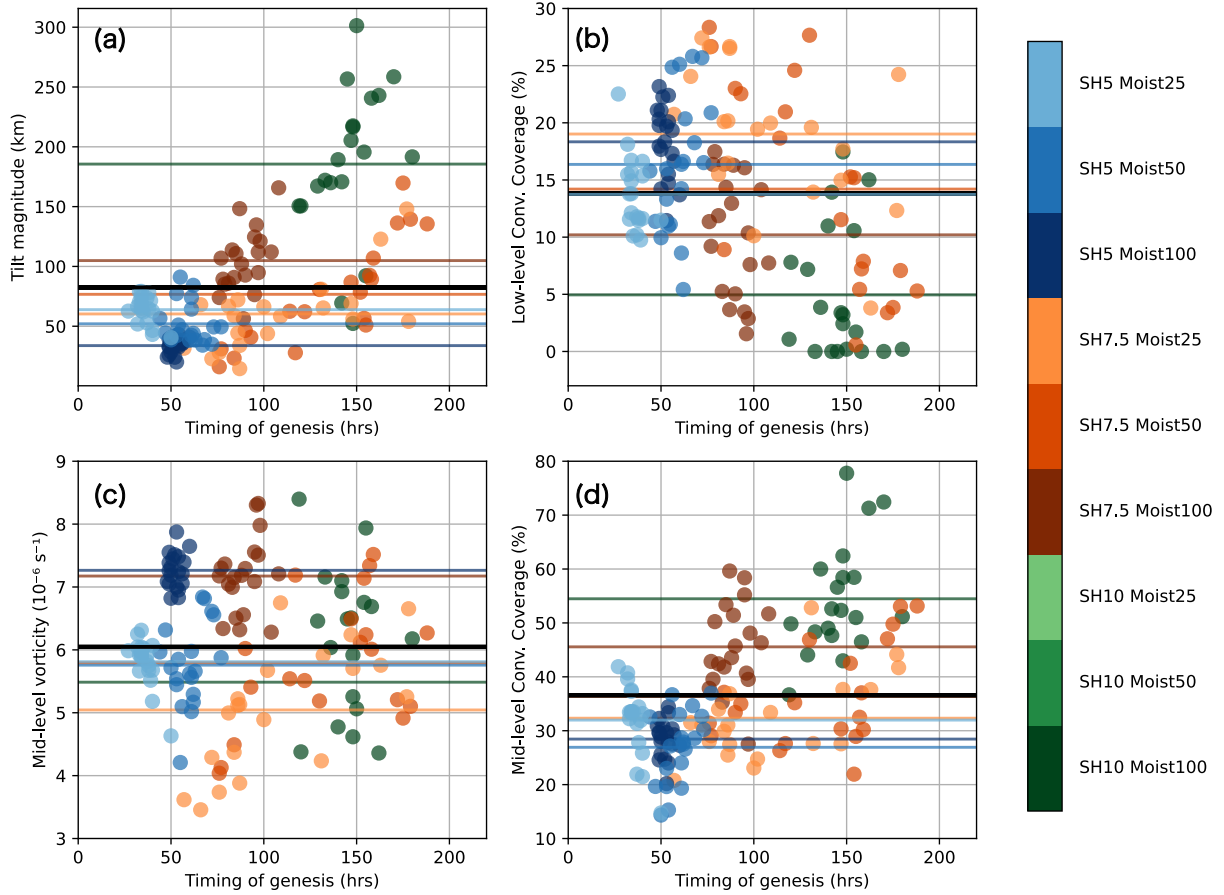
342 We found the difference between the earliest and latest developing members of the most uncer-
343 tain ensemble set (SH7.5_Moist50) was how many cycles of increasing convective coverage and
344 decreasing vortex tilt they go through to have a successful TC intensification. Now, our question
345 is whether there exist physical differences between the successful and unsuccessful cycles of these
346 precursor events. Due to the stochastic characteristic of convective initiation and complicated
347 multi-scale interactions between convection and the sheared environment (e.g., Nam and Bell
348 2021), the predictability of tropical cyclone intensification in this particular environment could be
349 limited when using deterministic methods. In response to this inherent uncertainty, we adopted a
350 probabilistic approach to quantify the number of precursor event trials necessary to achieve tropical
351 cyclone intensification in each ensemble member.

352 Our probabilistic approach is inspired by the statistical model of the geometric distribution,
353 which is the probability distribution of the number of Bernoulli trials needed to get one success.
354 A famous example would be how many trials of coin flipping are required to get the tail side of
355 the coin. In our case, each Bernoulli trial will be a precursor event, such as tilt decreasing below a
356 certain threshold, and the success is TC genesis (i.e., MSLP reaching 996 hPa). Bernoulli trials are
357 assumed to be independent, but we note that each precursor event cannot be purely independent of
358 the other; the vorticity or moisture produced by previous convective bursts primes the environment
359 for subsequent convective bursts. For example, the latest developing member of SH7.5_Moist50 had
360 a larger mid-level circulation and a lower SLP at the beginning of its fourth cycle compared to the
361 second cycle (Figs. 5, and 8). Therefore, we quantitatively assessed the importance of the repeated
362 trials of key physical processes leading to TC intensification, but because of the interdependence
363 of precursor events we did not directly fit the data to a geometric or other probability distribution.

364 We used four precursor variables of vortex tilt magnitude, inner-core average mid-level vorticity,
365 inner-core low-level convective coverage, and inner-core mid-level coverage to diagnose vortex
366 misalignment, vortex intensity, and convective organization. We set the threshold of each pre-
367 cursor variable as the mean value of the variable at the genesis timing for all 140 developing
368 members (except for 40 members of SH10_Moist50 and SH10_Moist25). The thresholds for the
369 four precursors of vortex tilt magnitude, inner-core average mid-level vorticity, inner-core low-level
370 convective coverage, and inner-core mid-level coverage are < 82.0 km, $> 6 \times 10^{-6} \text{ s}^{-1}$, > 14.0
371 %, and > 37.0 %, respectively (black lines in Fig. 9). We count it as a precursor event for each
372 variable when that variable passes the threshold for at least 3 hours. For example, if the vortex tilt
373 was above 82 km at hour H and decreased below 82 km at hour H+1, and the vortex tilt continued
374 to be below 82 km until hour H+3, we count it as a distinct tilt-decreasing precursor event.

375 The spread of data points of each precursor variable at genesis time indicates reaching a threshold
376 does not guarantee TC intensification (colored dots in Fig. 9). Our choice of threshold is a tool
377 to count the distinctive episodes of tilt decrease or convective bursts as shown in Fig. 3 for a
378 fair comparison for all developing ensemble members. We confirmed that the method of using
379 the median as a threshold instead of the mean did not affect the statistical results. We also tested
380 the sensitivity of statistics using different thresholds for each ensemble set (colored horizontal
381 lines in Fig. 9). The results were generally the same except for the SH10 ensemble sets because

382 SH10_Moist100 is the outlier having a larger tilt and mid-level convective coverage and smaller
 383 low-level coverage (see green dots and lines in Fig. 9).



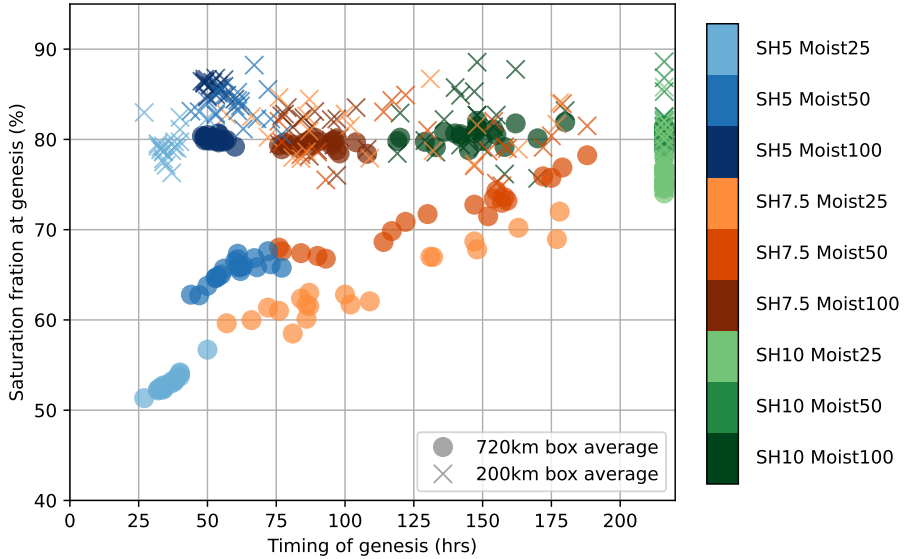
384 FIG. 9. The magnitude of the four TC intensification precursor variables of (a) vortex tilt magnitude, (b)
 385 low-level convective coverage, (c) average mid-level vorticity, and (d) mid-level convective coverage at genesis
 386 time for each ensemble member that underwent intensification during the 9-day simulation time. Horizontal lines
 387 indicate the average value for each color-coded ensemble set. The thicker black line is the average value of all 140
 388 ensemble members at genesis timing, which was used as the threshold to count the number of precursor events:
 389 82 km for vortex tilt, 14 % for low-level convective coverage, $6 \times 10^{-6} s^{-1}$ for inner core mid-level vorticity, and
 390 37 % for mid-level convective coverage.

391 We analyzed saturation fraction as a candidate for precursor variable for TC intensification
 392 because previous studies have shown that sufficient saturation fraction above 80-85 % is essential
 393 for TC genesis and intensification (Nolan et al. 2007; Raymond et al. 2014; Bell and Montgomery

394 2019). Figure 10 displays the saturation fraction at genesis time for all ensemble members of the
395 nine sets. Saturation fraction is calculated as the integrated mass-weighted mixing ratio divided by
396 the integrated mass-weighted saturation mixing ratio over the vertical layers between the surface
397 to 6 km (Raymond and Kilroy 2019).

398 We found the saturation fraction threshold varies a lot depending on the size of the computation
399 domain. The saturation fraction value at the timing of genesis varies from about 50 % to 80 % (for
400 720 km domain size) and from 75 % to 89 % (for 200 km domain size) depending on the shear and
401 humidity configurations. For the 720 km box average, among the dry sets (Moist50 and Moist25),
402 SH5 sets have the lowest saturation fraction, and SH10 sets have the highest domain average
403 saturation fraction. It appears that simulated TCs of the SH5_Moist50 and SH5_Moist25 sets
404 contain the moisture and heat energy in the inner-core region of the storm and utilize it efficiently
405 to spin up the vortex; whereas the drier sets, under VWS 10 m s^{-1} , have moisture spread over a
406 larger area shortly after it is produced by convective activities. Thus, the larger domain of the drier
407 sets of SH10 becomes moister and moister but the vortex cannot intensify, and pressure cannot
408 deepen. More importantly, a significant saturation fraction increase appears to occur after the
409 TC genesis for most of the ensembles (Supplemental Figs. 4-5), which means saturation fraction
410 increase follows TC genesis rather than leading to it. Thus, we did not use saturation fraction
411 increase as a precursor event. However, inner-core moistening occurred in the first 36 hours of
412 initial spinup for all ensemble members regardless of shear and moisture setup, and moistening the
413 inner-core can be a necessary condition that happens well before genesis. We did not examine the
414 asymmetric ventilation or moistening around the convective area (Alland et al. 2021a; Alvey and
415 Hazelton 2022), which may be more important for TC genesis than the domain averaged humidity.

420 Figure 11 shows the number of precursor events before TC genesis. A key takeaway from Fig. 11
421 is that the marginally favorable environments of SH7.5_Moist50 and SH7.5_Moist25 have the most
422 attempts of precursor events (up to 7 times) among all the experiments. Note that the precursor
423 events count based on the thresholds in Fig. 9 are different from how we subjectively annotated
424 the cycles of convective bursts from Fig. 3. For the Moist100 sets in the left column of Fig. 11,
425 the three sets show similar distributions for mid-level vorticity increase and low-level convective
426 coverage (Fig. 11c, e). For tilt decrease (Fig. 11a), all of the SH10_Moist100 and a majority of
427 SH7.5_Moist100 ensemble members reached the point of TC genesis with mid-level and low-level



416 FIG. 10. Domain-averaged saturation fraction at genesis versus time of genesis. Circles denote the saturation
 417 fraction averaged in the 720 km x 720 km box centered around the low-level vortex, and crosses are for the 200
 418 km x 200 km box centered around the low-level vortex. Data points of non-developing ensemble members of
 419 SH10_Moist25 and SH10_Moist50 are at hour 216.

428 vortex centers misaligned by farther than 82 km (Fig. 9a). Moist100 provides a very favorable
 429 thermodynamic setup of sea surface temperatures of 29°C and moist tropical sounding, thus, it is
 430 likely that simulated TCs under Moist100 can afford a larger magnitude of vortex tilt. Moist50
 431 and Moist25, on the other hand, have a region of drier air in the outer-core region that can easily
 432 be brought into the inner-core region through radial ventilation if the vortex tower is tilted (Fig.
 433 11b). Then, Fig. 11g shows that stronger VWS environments required more repetitions of mid-
 434 level convective coverage increasing beyond 37 %, implying a lower success rate of the mid-level
 435 convective bursts leading to TC intensification in a stronger VWS condition.

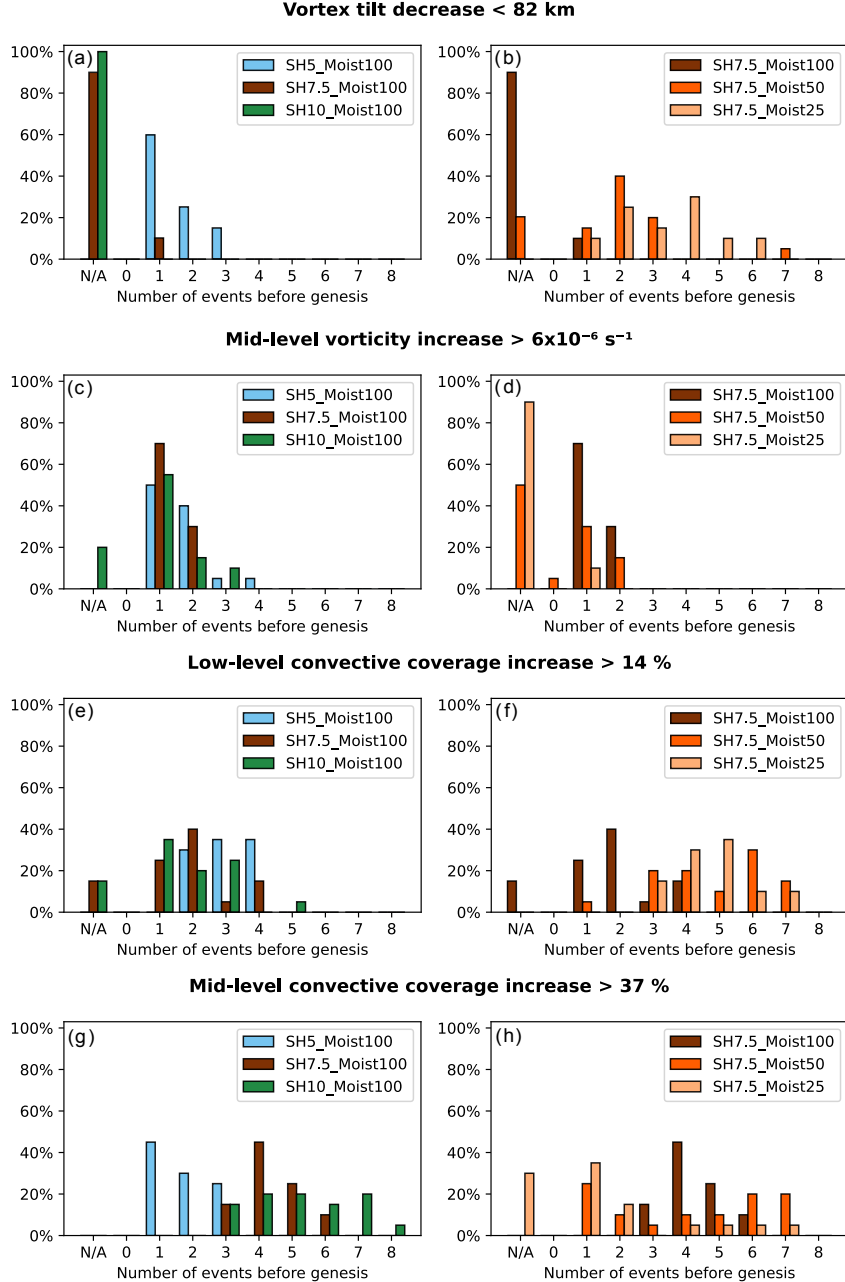
436 Among SH7.5 sets, it is the drier experiments that have the widest spread of the number of
 437 precursor events that are required to reach TC genesis (Fig. 11b, f, h). The wide spread of the
 438 number of precursor events for the ensemble sets having a combination of moderate VWS and dry
 439 air is directly related to uncertainties in predicting genesis time or intensification onset. Mid-level

440 vorticity increase, in general, has smaller numbers of attempts compared to the other variables
441 because averaged vorticity increases more gradually than episodically (c.f. Fig. 3).

448 Figure 12 displays the timing of the four precursor events against the timing of TC genesis for
449 each ensemble member. There are many overlaps of the circles in each panel of Fig. 12 because all
450 140 developing members are shown, and many of the members underwent more than one precursor
451 event before genesis. Vortex tilt decrease and low- and mid-level convective coverage increase
452 exhibit a repeated cycle (see the orange arrows moving upward on y-axis of Fig. 12). An initial
453 convective burst occurs in the first 24 hours of model spin-up time (Fig. 12b, d). The second cluster
454 of bursts occurs between 50-75 hours. Then the following episodes occur between 100-175 hour
455 (if TC genesis did not happen until that point). The timing of mid-level vorticity increase almost
456 coincides with the timing of genesis, only a few hours earlier. As discussed above, for vortex tilt,
457 the reason why there are no data points of SH7.5_Moist100 and SH10_Moist100 in these ensembles
458 reach TC genesis with vortex tilt larger than our threshold of 82 km (Fig. 9a). We conjecture that
459 the TCs in these two ensemble sets intensify relying on the favorable thermodynamic environments
460 despite the large magnitude of tilt (see large mid-level convective coverage in Fig. 9d and many
461 mid-level convective burst events in Fig. 11g for SH10_Moist100).

462 The precursor event that has the longest lead time before TC genesis appears to be mid-level
463 convective coverage increase, especially for SH7.5_Moist50 and SH7.5_Moist25, which are the
464 ensemble sets that have the widest ensemble spread (see the distance between y=x line and the
465 orange circles in Fig. 12). For SH7.5_Moist50 and SH7.5_Moist25, the latest occurrence of mid-
466 level convective coverage increasing beyond 37 % before TC genesis happens, on average, 31.4 and
467 34.4 hours prior to genesis time, respectively. On the other hand, the latest occurrence of low-level
468 convective coverage increasing beyond 14 % before genesis happens, on average, 15.6 and 8.7 hours
469 prior to genesis time for SH7.5_Moist50 and SH7.5_Moist25, respectively. It is consistent with
470 Fig. 3 that showed mid-level convective coverage has more persistence than low-level convective
471 coverage when tilt is amplifying again.

476 This section focused on analyzing the probabilistic characteristic of TC intensification under
477 marginally favorable environmental conditions. Our findings revealed that each simulation set
478 exhibited a unique distribution of precursor event cycles that a TC must undergo before intensifying.
479 The complex and chaotic nature of TC-VWS-dry air interactions, particularly around the convective



442 FIG. 11. Histograms of the number of TC genesis precursor events occurring before the timing of genesis.

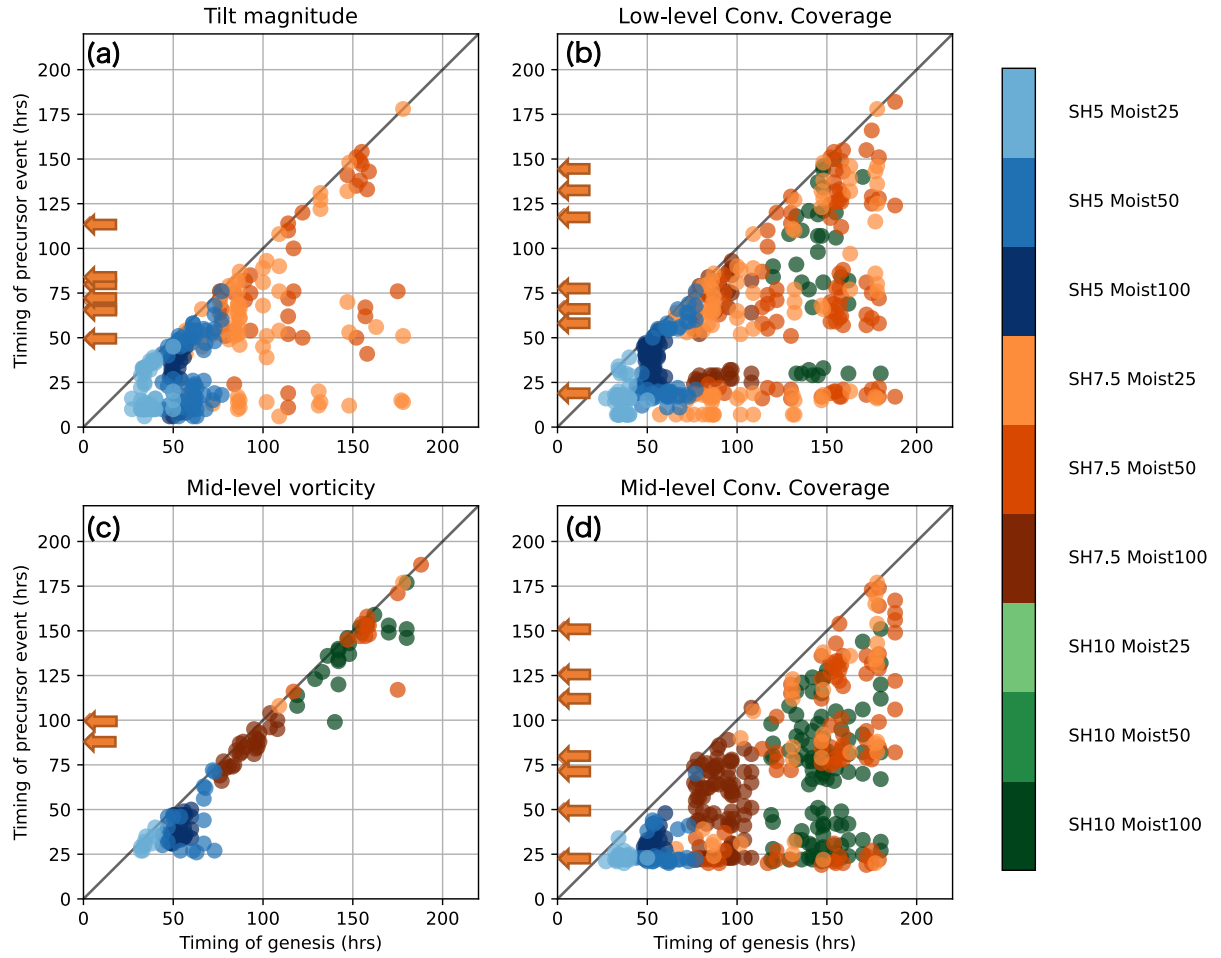
443 Histograms of (a), (c), (g), and (e) are for Moist100 simulations, composed by shear magnitude. Histograms

444 of (b), (d), (f), and (h) are for SH7.5 simulations, composed by environmental moisture magnitude. Each

445 event is counted with the precursor parameter keeping its value above/below the threshold (Fig. 9) for 3 hours

446 continuously. N/A (Not applicable) bin is for the simulations that reached genesis without surpassing the

447 thresholds for the precursor variables.



472 FIG. 12. Timing of the TC genesis precursor events compared to the timing of genesis. Each event is counted
 473 with the precursor parameter keeping its value above/below the threshold (Fig. 9) for 3 hours continuously. The
 474 orange arrows indicate the median time of the first, second, ..., and 7th (if any) precursor events for 60 members
 475 of the three SH7.5 sets.

480 bursts and the vortex alignment process, was evident in these results. However, we also observed
 481 a consistent and steady increase in accumulated vorticity and column saturation fraction. These
 482 results demonstrate the multifaceted and intricate mechanisms involved in TC intensification under
 483 moderately sheared and dry environments.

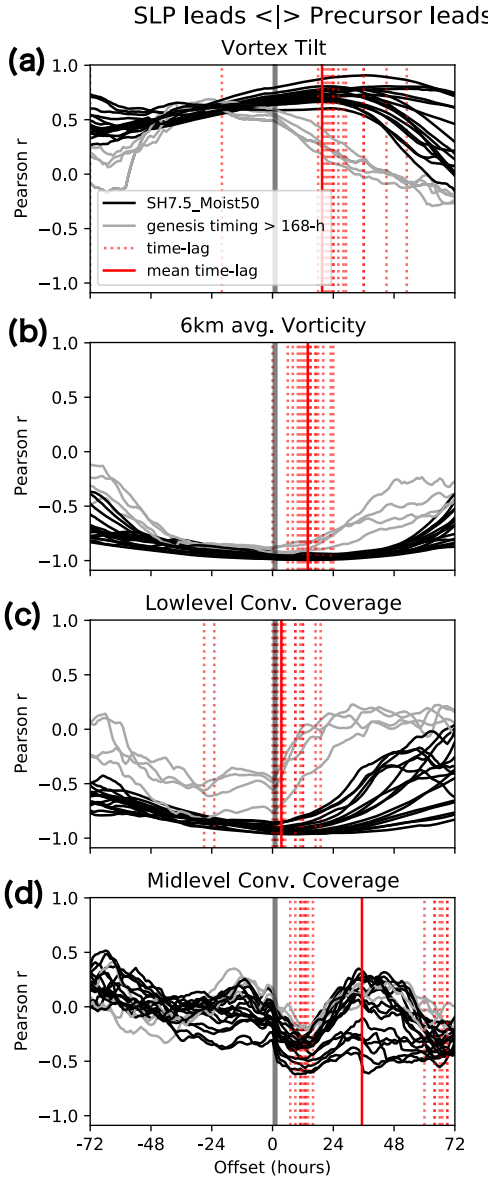
484 *d. Time-lagged correlation analysis*

485 The different distribution of the timing of each precursor event before the timing of genesis
486 (Fig. 12) warrants a further investigation of the time order among the physical processes that are
487 represented by the precursor variables. Here we present time-lagged cross-correlation analysis
488 results. Time-lagged cross-correlation refers to the correlation between two time series that are
489 shifted in time relative to one another.

490 Figure 13 shows time-lagged correlations between the time series of 217 hours of hourly MSLP
491 and the precursor variables (vortex tilt, mid-level inner-core average vorticity, and low- and mid-
492 level inner-core convective coverage) of the 20 ensembles of SH7.5_Moist50. Vortex tilt should
493 have a positive correlation with MSLP, for tilt decreases as MSLP decreases. Vorticities and
494 convective coverages should have a negative correlation with MSLP because they increase as
495 MSLP drops. Shifting the time series hour by hour, we can find a time-lag that records a maximum
496 (vortex tilt) or minimum (vorticity and convective coverage) correlation with MSLP (red dotted
497 lines in Fig. 13). The red solid line denotes the mean time-lag from 16 members of SH7.5_Moist50.
498 Four members that have TC genesis after 168 hours were excluded to ensure at least 48 hours offset
499 from the end of simulation hours given the -72 – +72 hours offset kernel (grey lines in Fig. 13).

500 Positive time-lag means the time series of the precursor variable leads the time series of MSLP,
501 which implies predictability for TC intensification. Among the four precursor variables, mid-level
502 convective coverage has the longest mean lead time. However, mid-level convective coverage has
503 a larger variance from member to member compared to the other three variables, which could
504 be interpreted as a less reliable predictor. The reason why the time-lag of mid-level convective
505 coverage and MSLP has a large variance is because these time-lagged correlations (Fig. 13d) have
506 two distinctive modes at around 12 hours and 72 hours of lead time, unlike the other variables
507 that have a single peak (vortex tilt) or a single trough (mid-level vorticity and low-level convective
508 coverage). Among the four variables in Fig. 13, the mid-level vorticity has the best correlation and
509 the narrowest spread of the time-lag for SH7.5_Moist50 ensembles, but it has a shorter mean lead
510 time of 12 hours.

511 The wave-like pattern (multiple peaks and troughs) of cross-correlations between mid-level
512 convective coverage and SLP is found not only from SH7.5_Moist50 ensemble members but also
513 from other ensembles (Fig. 14). The wavy pattern is thought to be related to multiple incidences of



511 FIG. 13. Time-lagged Pearson correlations between time series of minimum sea level pressure (MSLP) and
 512 (a) vortex tilt, (b) mid-level vorticity, (c) low-level convective coverage, (d) mid-level convective coverage for
 513 the SH7.5_Moist50 experimental set. Red dotted vertical lines indicate the time-lag of maximum/minimum
 514 correlation for each ensemble member. Red solid lines indicate the mean time-lag for the members with genesis
 515 timing \leq 168 hours. Positive time-lag means each precursor event happens before SLP drops below 996 hPa
 516 threshold and vice versa.

convective bursts. For some members, the two or more local minima of correlations have similar values such that identifying the time-lag becomes somewhat uncertain (Fig. 14e,f). Comparing the 3x3 panels in Fig. 14, there is a trend that the ensembles from more favorable setups (e.g., SH5_Moist100) have a longer lead time of the mid-level convective coverage, better correlation, and a narrower ensemble spread. On the contrary, the ensemble that had the widest spread in SLP (i.e., SH7.5_Moist50) also exhibits a large ensemble spread in time-lag distributions. The 3x3 figures like Fig. 14 for the three other precursor variables can be found in Supplemental Figs. 1-3 and they show similar patterns as Fig. 13a-c with a single peak or trough.

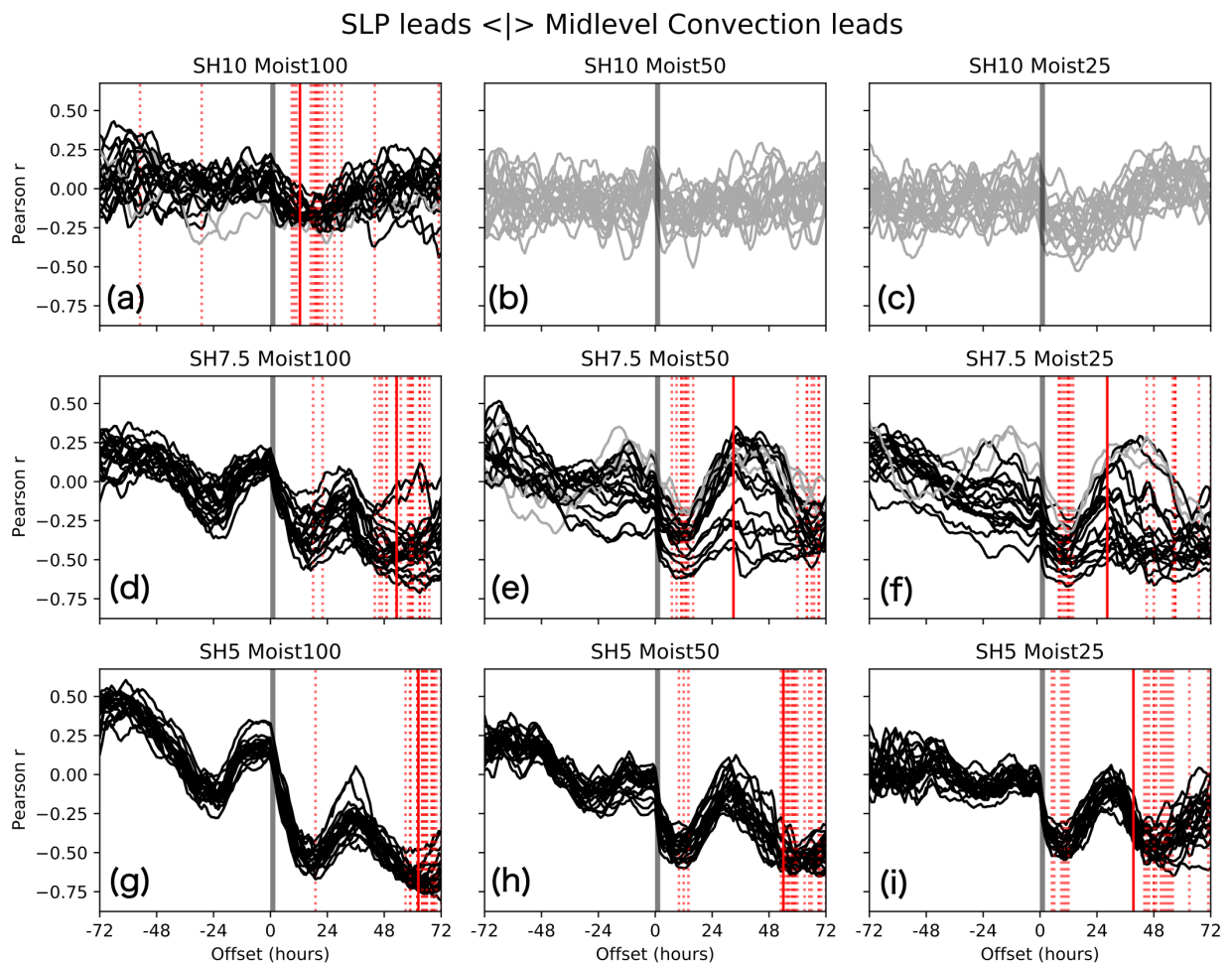


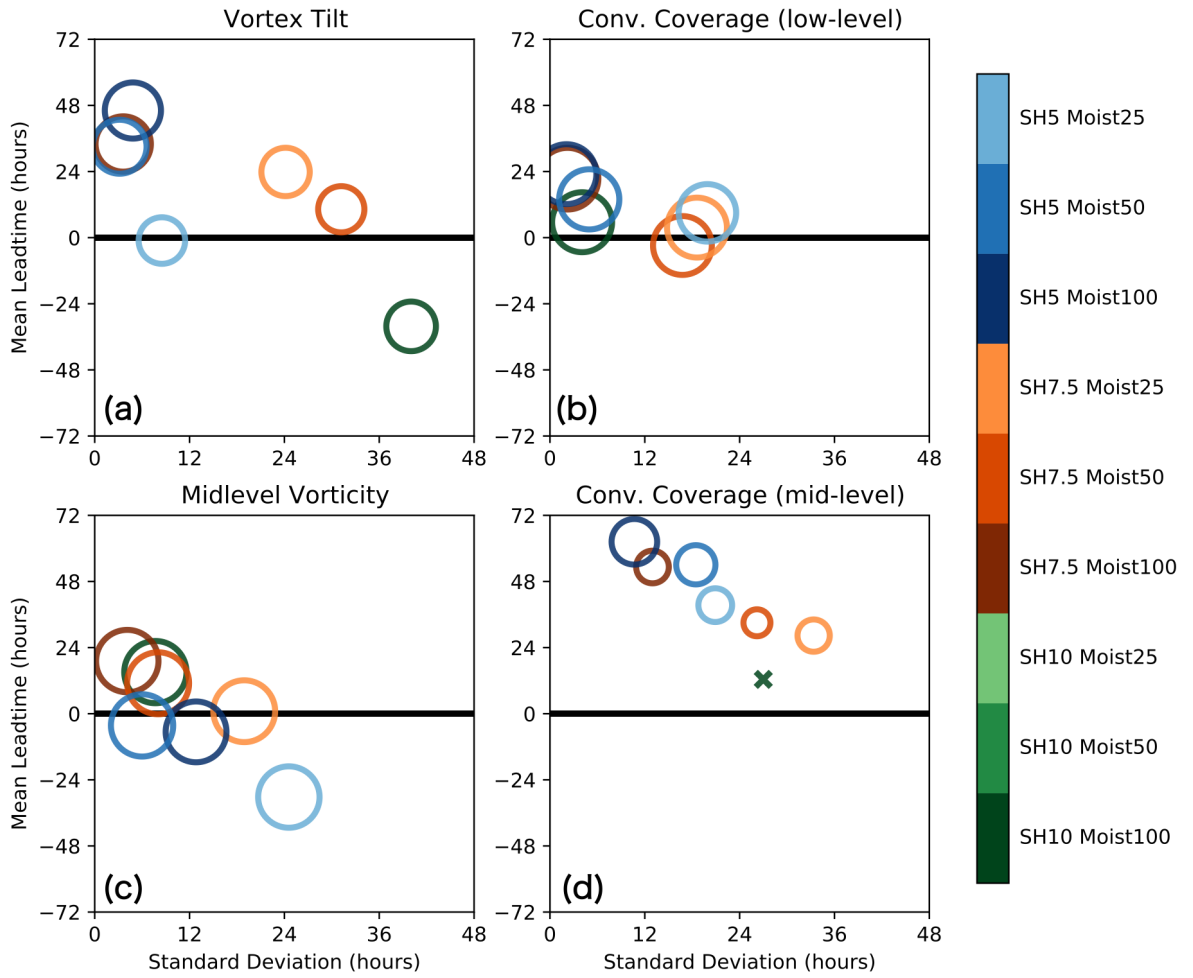
FIG. 14. Time-lag Pearson correlation between time series of minimum sea level pressure (MSLP) and mid-level convective coverage as a function of time-lag for the whole 9 sets of experiments. Annotation is the same as Fig. 13.

531 Figure 15 summarizes the results of time-lagged cross-correlation analysis for all four precursor
532 variables in one plot. The ensemble-mean time-lag is on the y-axis, and the standard deviation
533 of the time-lags is on the x-axis, such that the upper-left corner denotes the best predictor for TC
534 intensification with a long lead time and good confidence. The marker size is proportional to the
535 ensemble mean time-lagged correlation value. Some ensemble members of SH10_Moist100 did
536 not have a statistically significant correlation between mid-level convective coverage and MSLP at
537 95 % confidence level based on a two-sided Student's t-test, thus it is marked with 'x' instead of
538 'o' (see Figs. 14 a and 15 d).

539 In Fig. 15, we observe that the more favorable setups, characterized by smaller VWS and
540 moister environments, generally exhibit metrics with longer lead times, less spread, and better
541 correlations with MSLP evolution, in general. Among the four variables of precursor events, the
542 order of mean lead time is 1) mid-level convective coverage, 2) vortex tilt, 3) low-level convective
543 coverage, and 4) mid-level vorticity. The longer lead time, the smaller correlation, and the larger
544 standard deviation of the mid-level convective coverage with MSLP imply that mid-level convective
545 coverage increasing (that usually happens 48 hours before TC genesis) does not always end up with
546 TC intensification. Higher correlation and smaller ensemble spread of mid-level vorticity mean
547 that mid-level vorticity increasing (that usually happens 12 hours before TC genesis) has a better
548 chance of resulting in imminent TC intensification compared to mid-level convective coverage
549 increasing. However, it is important to note that despite these statistical trends, our analyses have
550 revealed overlaps between circles and similar lead times for different variables, as depicted in both
551 Figs. 12 and 15. This analysis indicates that the time order of these precursor events is not easily
552 separable and highlights the uncertainties in causal relationships leading to TC intensification. The
553 time order of each precursor event and the probability of each precursor event eventually leading
554 to TC intensification are further discussed in section 4.

560 4. Discussion and Conclusions

561 Our extensive mesoscale ensemble modeling demonstrates that marginally favorable envi-
562 ronments, characterized by moderate magnitudes of VWS and intermediate levels of humidity
563 (SH7.5_Moist50 and SH7.5_Moist25), are associated with the highest level of uncertainty in tropi-
564 cal cyclone genesis and intensification, consistent with previous literature (Alland et al. 2021a; Tao

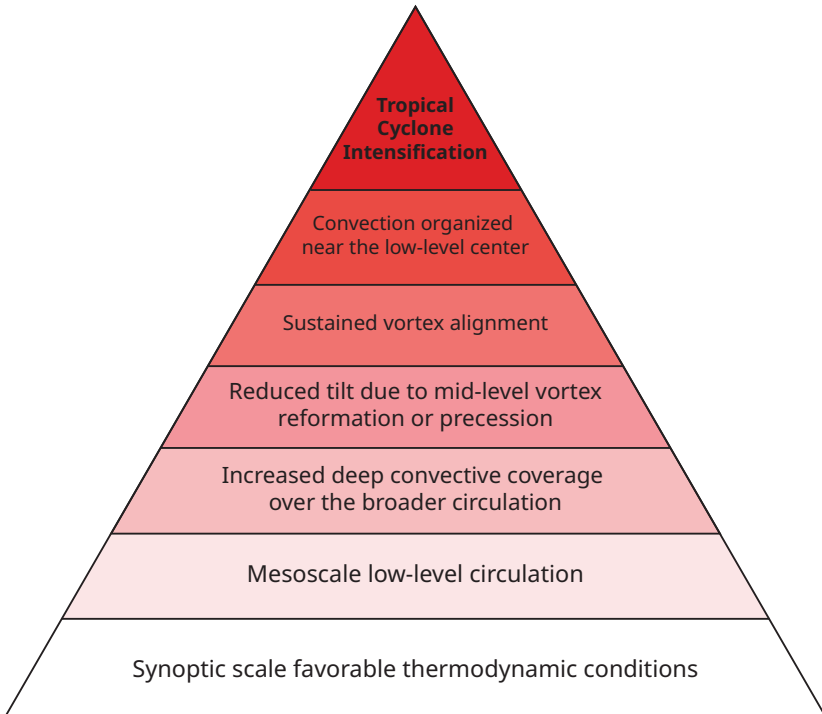


555 FIG. 15. Time-lag correlation analysis results for the time series of minimum sea level pressure (MSLP) and
 556 each of the four precursor variables with a mean of time-lag for the y-axis and standard deviation of the time-lag
 557 of 20 ensemble members in the x-axis. The size of the circle is proportional to the mean correlation between
 558 two time series at the time-lag. The combination that had a correlation not significant at 95% level is marked
 559 with ‘x’ rather than a circle. The ensemble sets that do not have any developing members are not shown.

565 and Zhang 2014). A key finding was that there are repetitive cycles of precursor events lining up
 566 together before TC intensification, and slow or non-developing ensemble members of the marginal
 567 environments go through a number of the cycles of precursor events that are very close to successful
 568 ones.

569 Based on the close examination of selected ensemble members and statistical analysis of prob-
 570 abilities of precursor events and time-lagged correlations, we propose a diagram that represents

571 the hierarchy of the processes leading into tropical cyclone intensification in sheared and dry
572 environments (Fig. 16).



573 FIG. 16. A pyramid diagram of tropical cyclone (TC) intensification in moderately sheared and dry environ-
574 ments. The diagram shows the hierarchy of the precursor events leading to TC intensification for a lower floor
575 condition should be satisfied for the TC to move on to the next upper floor of the pyramid. There could be multiple
576 trials to satisfy the condition on each floor and TCs can climb up the pyramid to go closer to intensification onset
577 or descend and move further away from the pinnacle.

578 The first floor of the pyramid in Fig. 16 is synoptic scale favorable thermodynamic conditions.
579 Gray (1979) showed that a moist atmosphere and a well-mixed, warm oceanic layer serve as
580 necessary conditions for TC genesis. We prescribed warm SSTs of 29 °C, and all 180 simulations
581 spent the first 24–36 hours of incubation time to moisten the inner-core region (Fig. 10). The second
582 floor is the existence of closed mesoscale low-level circulation. We initialized the simulations with
583 a weak vortex centered at 850 hPa. Low-level closed circulation is one of the first signals of
584 intensification found from tropical disturbances in the range of 'Invest' and TD (Nam and Bell
585 2021; Wang et al. 2012). After the first two floors set the stage for synoptic to meso-alpha scale

environments, on the third floor, there emerges a wider area of deep convection (captured by increasing signals of mid-level and low-level convective coverage parameters). Inside the deep organized mesoscale convective system, a new mid-level vortex forms inside the broader pre-existing mid-level circulation (Fig. 7), which results in rapid vortex tilt decrease: the fourth floor of the pyramid. The fifth floor is sustained vertical alignment of the newly reformed mid-level vortex and the low-level vortex. If the newly reformed mid-level vortex becomes firmly aligned with the low-level vortex, the vortex tower can be resilient against VWS (Schecter and Montgomery 2003; Reasor et al. 2004). In our analysis, the vortex alignment process manifests as the tilt keeps decreasing with some fluctuation (e.g., 100-125 hours of the early-developing member and 150-175 hours of the late-developing member from SH7.5_Moist50 in Fig. 3). If the fifth floor was successful, vortex tilt keeps decreasing, and the deep convection that is centered around the mid-level center organizes itself near the low-level center: the sixth floor. Then, the mid-level vortex intensifies, as captured by mid-level vorticity increasing, and the simulated vortex finally reaches the pinnacle of the pyramid and the TC intensifies.

In this study, we expand our knowledge of the dynamic and thermodynamic processes that lead to TC intensification in sheared and dry environments by showing the probabilistic distribution of the precursor events and identifying the critical processes that serve as the bifurcation points between the developing and non-developing vortices in the course of the repetitive cycles of precursor events. The ensemble sets that have a narrower ensemble spread (small VWS and high humidity) need only a few cycles of precursor events, but the ensemble sets that have a wider ensemble spread have some members developing after one or two cycles and other members developing after seven to eight cycles of precursor events repeating with a 24-48 hours period (Fig. 11). We suggest that the widespread distribution of the number of precursor events is related to the lower success rate of each precursor event. Whether each cycle of precursor events is successful for TC genesis or not is somewhat random due to the stochastic characteristic of convective scale phenomena, but the probability of success of each cycle can increase with time as the environment becomes moister and more favorable with each cycle (Fig. 5 vs. Fig. 8).

The critical bifurcation point in these experiments appears to be the fifth floor of the pyramid, the sustained vortex alignment process, for SH7.5_Moist50 and SH7.5_Moist25 set. Before TC genesis, mid-level convective coverage increases, and vortex tilt decreases multiple times (Fig. 12).

616 These variables have a longer lead time with a smaller correlation and larger standard deviation
617 (Fig. 15). This means that not all events of mid-level convective coverage increasing and vortex
618 tilt decreasing result in low-level convective coverage increasing or mid-level vorticity increasing.
619 From these results, we infer that most of the late-developing members of SH7.5_Moist50 fail
620 at the sustained vortex alignment process; there is a newly reformed meso-beta scale mid-level
621 vortex close to the existing meso-alpha scale low-level center, but the mid-level vortex is advected
622 downshear swiftly before the vortices in different vertical layers align and grow resilient against
623 VWS. Then, the vortex tilt increases again, and the cycle resets, going back to the third floor of the
624 pyramid again. While our statistical and probabilistic analyses provide insights into the time order
625 of events, the overlaps in the lead-time and large variances also demonstrate the intricate challenges
626 of disentangling the precise timing and causal relationships between the various precursor events.

627 We could not pinpoint the difference between the mid-level vortex that can maintain sustained
628 vortex alignment with the low-level vortex versus the ones that are carried away. We looked at the
629 location of deep convection in shear quadrants, the location of the newly formed mid-level vortex
630 with regard to the low-level vortex center, and stratiform coverage (see Supplemental Fig. 6), but
631 some cases exhibited very similar patterns, yet one underwent TC genesis and the other failed.
632 Nevertheless, we can infer from saturation fraction analysis and mid-level vortex cross-sections
633 that a mid-level vortex that is formed closer to the low-level center with a larger spatial scale
634 and a more moist environment helps sustain the vortex alignment process. We observed cyclonic
635 movement of deep convection from the downshear to downshear-left direction prior to the rapid
636 decrease in tilt for both the earliest and latest developing members (Supplemental Fig. 6). This
637 observation is consistent with previous studies (e.g., Rios-Berrios et al. 2018), suggesting that the
638 asymmetric distribution of moisture and convection relative to shear direction could be another
639 significant distinction between developers and non-developers. Additional research is required to
640 better understand the factors that lead to sustained vortex alignment in the presence of VWS and
641 dry air.

642 This research aimed to identify the sources of increased uncertainty of tropical cyclone inten-
643 sification in marginally favorable environments through the understanding of the key multi-scale
644 precursors leading to tropical cyclogenesis and intensification in such environments. Based on the
645 results herein, the uncertainty can be largely attributed to the probabilistic characteristics of pre-

cursor events lining up together before TC genesis and intensification. In an extremely favorable or hostile environment, the success rate of each precursor event is either very high or very low, so the probability of ultimate TC intensification is skewed to 1 or 0. However, in a marginal environment, the success rate is moderate such that a TC can undergo TC genesis and continuous intensification with a first trial, or it could exhibit robust signals such as deep convective organization or low-level closed circulation but still fail to intensify. In reality, the environmental conditions change, thus a system that requires multiple repetitions of precursor events could miss the window of opportunity and dissipate as the environment becomes more hostile. On the other hand, some systems could develop into a TC climbing up the pyramid rapidly after entering a more favorable environment like the case of Hagupit (2008) (Nam and Bell 2021).

Our idealized simulations simplify the variable space by having the other variables constant to isolate the impacts of varying VWS and environmental humidity. In reality, there is a lot more complexity that contributes to the uncertainty around TC genesis and intensification, such as land-TC interaction (Alvey et al. 2022). We conducted additional experiments to investigate sensitivity to different types of the initial vortex (mid-level centered and weaker vortex) and choices of radiation and microphysics schemes (long and short wave radiation and Thompson microphysics). The preliminary analysis of these sensitivity test experiments showed that all successfully developing TCs shared these common precursor events as described in Fig. 16 while the critical bifurcation points of success and failed intensification cases were different depending on the experiments. For example, mid-level centered vortices in 7.5 m s^{-1} of VWS and Moist50 setups had an even larger ensemble spread than the low-level centered vortices in SH7.5_Moist50 shown here, and the late-developing members of the mid-level sensitivity test failed at the mid-level vortex reformation process (fourth floor of the diagram) not the sustained alignment process (fifth floor of the diagram). Our findings from the sensitivity tests will be reported in a subsequent study, which will continue to bridge the gap between the idealized simulations shown herein and the more complex reality of the tropical atmosphere.

672 *Acknowledgments.* The authors thank Eric Maloney, Steve Rutledge, Brian Tang and two anonymous
673 reviewers for their helpful comments. This research was funded by Office of Naval Research
674 awards N000141613033 and N000142012069. Computational resources were provided by XSEDE
675 allocation TG-ATM190001.

676 *Data availability statement.* The high resolution model outputs that support the findings of this
677 study are too large and stored in local computer clusters, thus are only available on request from
678 the corresponding author, CCN, but the key input files to reproduce the simulations are available
679 at <https://doi.org/10.5281/zenodo.6476490>.

680 References

- 681 Alland, J. J., B. H. Tang, and K. L. Corbosiero, 2017: Effects of midlevel dry air on development
682 of the axisymmetric tropical cyclone secondary circulation. *J. Atmos. Sci.*, <https://doi.org/10.1175/JAS-D-16-0271.1>.
- 684 Alland, J. J., B. H. Tang, K. L. Corbosiero, and G. H. Bryan, 2021a: Combined effects of midlevel
685 dry air and vertical wind shear on tropical cyclone development. Part I: Downdraft ventilation.
686 *J. Atmos. Sci.*, **78** (3), 763 – 782, <https://doi.org/10.1175/JAS-D-20-0054.1>.
- 687 Alland, J. J., B. H. Tang, K. L. Corbosiero, and G. H. Bryan, 2021b: Combined effects of midlevel
688 dry air and vertical wind shear on tropical cyclone development. Part II: Radial ventilation. *J.*
689 *Atmos. Sci.*, **78** (3), 783 – 796, <https://doi.org/10.1175/JAS-D-20-0055.1>.
- 690 Alvey, G. R., M. Fischer, P. Reasor, J. Zawislak, and R. Rogers, 2022: Observed processes
691 underlying the favorable vortex repositioning early in the development of Hurricane Dorian
692 (2019). *Mon. Wea. Rev.*, **150** (1), 193 – 213, <https://doi.org/10.1175/MWR-D-21-0069.1>.
- 693 Alvey, G. R., and A. Hazelton, 2022: How do weak, misaligned tropical cyclones evolve toward
694 alignment? a multi-case study using the hurricane analysis and forecast system. *J. Geophys. Res.*
695 *Atmos.*, **127** (20), e2022JD037268, <https://doi.org/10.1029/2022JD037268>.
- 696 Bell, M. M., and M. T. Montgomery, 2019: Mesoscale processes during the genesis of hurricane
697 Karl (2010). *J. Atmos. Sci.*, **76** (8), 2235–2255, <https://doi.org/10.1175/JAS-D-18-0161.1>.

- 698 Bhatia, K. T., and D. S. Nolan, 2013: Relating the skill of tropical cyclone intensity forecasts
699 to the synoptic environment. *Wea. Forecasting*, **28** (4), 961 – 980, <https://doi.org/10.1175/WAF-D-12-00110.1>.
- 700
- 701 Bracken, W. E., and L. F. Bosart, 2000: The role of synoptic-scale flow during tropical cyclogenesis
702 over the North Atlantic ocean. *Mon. Wea. Rev.*, **128** (2), 353–376, [https://doi.org/10.1175/1520-0493\(2000\)128<0353:TROSSF>2.0.CO;2](https://doi.org/10.1175/1520-0493(2000)128<0353:TROSSF>2.0.CO;2).
- 703
- 704 Chavas, D. R., K. A. Reed, and J. A. Knaff, 2017: Physical understanding of the tropical cyclone
705 wind-pressure relationship. *Nat. Commun.*, **8**, 1360.
- 706
- 707 Chen, X., Y. Wang, J. Fang, and M. Xue, 2018: A Numerical Study on Rapid Intensification
708 of Typhoon Vicente (2012) in the South China Sea. Part II: Roles of Inner-Core Processes. *J. Atmos. Sci.*, **75** (1), 235–255, <https://doi.org/10.1175/JAS-D-17-0129.1>.
- 709
- 710 Courtney, J., and J. A. Knaff, 2009: Adapting the knaff and zehr wind-pressure relationship
711 for operational use in tropical cyclone warning centres. *Aust. Meteorol. Oceanogr. J.*, **58**(3),
167–179.
- 712
- 713 Davis, C. A., and D. A. Ahijevych, 2013: Thermodynamic environments of deep convection
714 in Atlantic tropical disturbances. *J. Atmos. Sci.*, **70** (7), 1912–1928, <https://doi.org/10.1175/JAS-D-12-0278.1>.
- 715
- 716 Dunion, J. P., 2011: Rewriting the climatology of the tropical North Atlantic and caribbean sea
atmosphere. *J. Climate*, **24**, 893–908.
- 717
- 718 Dunion, J. P., and C. S. Marron, 2008: A reexamination of the Jordan mean tropical sounding
719 based on awareness of the Saharan Air Layer: Results from 2002. *J. Climate*, **21** (20), 5242 –
5253, <https://doi.org/10.1175/2008JCLI1868.1>.
- 720
- 721 Dunion, J. P., C. D. Thorncroft, and C. S. Velden, 2014: The tropical cyclone diurnal cycle of mature
hurricanes. *Mon. Wea. Rev.*, **142** (10), 3900 – 3919, <https://doi.org/10.1175/MWR-D-13-00191.1>.
- 722
- 723 Finocchio, P. M., and S. J. Majumdar, 2017: The predictability of idealized tropical cyclones in
724 environments with time-varying vertical wind shear. *J. Adv. Model. Earth Syst.*, **9** (8), 2836–2862,
725 <https://doi.org/10.1002/2017MS001168>.

- 726 Gray, W. M., 1979: *Hurricanes: Their Formation, Structure and likely Role in the Tropical*
727 *Circulation*, 155–218. James Glaisher House.
- 728 Hong, S.-Y., J. Dudhia, and S.-H. Chen, 2004: A revised approach to ice microphysical processes
729 for the bulk parameterization of clouds and precipitation. *Mon. Wea. Rev.*, **132**, 103–120.
- 730 Hong, S.-Y., Y. Noh, and J. Dudhia, 2006: A new vertical diffusion package with an explicit
731 treatment of entrainment processes. *Mon. Wea. Rev.*, **134**, 2318–2341.
- 732 James, R. P., and P. M. Markowski, 2010: A numerical investigation of the effects of dry air aloft on
733 deep convection. *Mon. Wea. Rev.*, **138** (1), 140 – 161, <https://doi.org/10.1175/2009MWR3018.1>.
- 734 Judt, F., S. S. Chen, and J. Berner, 2016: Predictability of tropical cyclone intensity: scale-
735 dependent forecast error growth in high-resolution stochastic kinetic-energy backscatter ensem-
736 bles. *Quart. J. Roy. Meteor. Soc.*, **142** (694), 43–57, <https://doi.org/10.1002/qj.2626>.
- 737 Klotzbach, P. J., M. M. Bell, S. G. Bowen, E. J. Gibney, K. R. Knapp, and C. J. Schreck,
738 2020: Surface pressure a more skillful predictor of normalized hurricane damage than
739 maximum sustained wind. *Bull. Amer. Meteor. Soc.*, **101** (6), E830 – E846, <https://doi.org/10.1175/BAMS-D-19-0062.1>.
- 740 Knaff, J. A., and R. M. Zehr, 2007: Reexamination of tropical cyclone pressure wind relationships.
741 *Wea. Forecasting*, **22**(1), 71–88.
- 742 Lorenz, E. N., 1969: The predictability of a flow which possesses many scales of motion. *Tellus*,
743 **21** (3), 289–307, <https://doi.org/10.1111/j.2153-3490.1969.tb00444.x>.
- 744 Martinez, J., C. C. Nam, and M. M. Bell, 2020: On the contributions of incipient vortex circulation
745 and environmental moisture to tropical cyclone expansion. *J. Geophys. Res. Atmos.*, **125** (21),
746 e2020JD033324, <https://doi.org/10.1029/2020JD033324>.
- 747 Melhauser, C., and F. Zhang, 2012: Practical and intrinsic predictability of severe and convective
748 weather at the mesoscales. *J. Atmos. Sci.*, 3350–3371.
- 749 Montgomery, M. T., and Coauthors, 2012: The pre-depression investigation of cloud-systems in
750 the tropics (PREDICT) experiment: Scientific basis, new analysis tools, and some first results.
751 *Bull. Amer. Meteor. Soc.*, <https://doi.org/10.1175/BAMS-D-11-00046.1>.

- 753 Moon, Y., and D. S. Nolan, 2010: Do gravity waves transport angular momentum away from
754 tropical cyclones? *J. Atmos. Sci.*, **67**, 117–135.
- 755 Murthy, V. S., and W. R. Boos, 2018: Role of surface enthalpy fluxes in idealized simula-
756 tions of tropical depression spinup. *J. Atmos. Sci.*, **75**, 1811–1831, <https://doi.org/10.1175/JAS-D-17-0119.1>.
- 758 Nam, C. C., 2021: Multi-scale interactions leading to tropical cyclogenesis in sheared environ-
759 ments. Ph.D. thesis, Colorado State University.
- 760 Nam, C. C., and M. M. Bell, 2021: Multiscale shear impacts during the genesis of Hagupit (2008).
761 *Mon. Wea. Rev.*, **149** (2), 551 – 569, <https://doi.org/10.1175/MWR-D-20-0133.1>.
- 762 Nguyen, L. T., and J. Molinari, 2015: Simulation of the downshear reformation of a tropical
763 cyclone. *J. Atmos. Sci.*, **72** (12), 4529–4551, <https://doi.org/10.1175/JAS-D-15-0036.1>.
- 764 Nguyen, L. T., J. Molinari, and D. Thomas, 2014: Evaluation of tropical cyclone center identifi-
765 cation methods in numerical models. *Mon. Wea. Rev.*, **142** (11), 4326 – 4339, <https://doi.org/10.1175/MWR-D-14-00044.1>.
- 767 Nolan, D., and M. McGauley, 2012: *Tropical cyclogenesis in wind shear: Climatological relation-
768 ships and physical processes*, 1–36. Nova Science Publishers, Inc.
- 769 Nolan, D. S., E. D. Rappin, and K. A. Emanuel, 2007: Tropical cyclogenesis sensitivity to
770 environmental parameters in radiative–convective equilibrium. *Quart. J. Roy. Meteor. Soc.*, **133**,
771 2085–2107, <https://doi.org/10.1002/qj.170>.
- 772 Ooyama, K. V., 1982: Conceptual evolution of the theory and modeling of the tropical cyclone. *J.
773 Meteor. Soc. Japan*, https://doi.org/10.2151/jmsj1965.60.1_369.
- 774 Peng, M. S., B. Fu, T. Li, and D. E. Stevens, 2012: Developing versus nondeveloping disturbances
775 for tropical cyclone formation. Part I: North Atlantic. *Mon. Wea. Rev.*, **140** (4), 1047–1066,
776 <https://doi.org/10.1175/2011MWR3617.1>.
- 777 Raymond, D. J., S. Gjorgjievska, S. Sessions, and Željka Fuchs, 2014: Tropical cyclogenesis and
778 mid-level vorticity. *Aust. Meteorol. Oceanogr. J.*, **64** (1), 11–25.

- 779 Raymond, D. J., and G. Kilroy, 2019: Control of convection in high-resolution simulations of
780 tropical cyclogenesis. *J. Adv. Model. Earth Syst.*, **11** (6), 1582–1599, <https://doi.org/10.1029/2018MS001576>.
- 782 Reasor, P. D., M. T. Montgomery, and L. D. Grasso, 2004: A new look at the problem of tropical
783 cyclones in vertical shear flow: Vortex resiliency. *J. Atmos. Sci.*, **61** (1), 3 – 22, [https://doi.org/10.1175/1520-0469\(2004\)061<0003:ANLATP>2.0.CO;2](https://doi.org/10.1175/1520-0469(2004)061<0003:ANLATP>2.0.CO;2).
- 785 Riemer, M., M. T. Montgomery, and M. E. Nicholls, 2010: A new paradigm for intensity modi-
786 fication of tropical cyclones: thermodynamic impact of vertical wind shear on the inflow layer.
787 *Atmospheric Chem. Phys.*, **10** (7), 3163–3188, <https://doi.org/10.5194/acp-10-3163-2010>.
- 788 Rios-Berrios, R., 2020: Impacts of radiation and cold pools on the intensity and vortex tilt of
789 weak tropical cyclones interacting with vertical wind shear. *J. Atmos. Sci.*, **77** (2), 669 – 689,
790 <https://doi.org/10.1175/JAS-D-19-0159.1>.
- 791 Rios-Berrios, R., C. A. Davis, and R. D. Torn, 2018: A hypothesis for the intensification of tropical
792 cyclones under moderate vertical wind shear. *J. Atmos. Sci.*, **75** (12), 4149–4173, <https://doi.org/10.1175/JAS-D-18-0070.1>.
- 794 Rios-Berrios, R., and R. D. Torn, 2017: Climatological analysis of tropical cyclone intensity
795 changes under moderate vertical wind shear. *Mon. Wea. Rev.*, **145** (5), 1717–1738, <https://doi.org/10.1175/MWR-D-16-0350.1>.
- 797 Rios-Berrios, R., R. D. Torn, and C. A. Davis, 2016: An ensemble approach to investigate tropical
798 cyclone intensification in sheared environments. Part II: Ophelia (2011). *J. Atmos. Sci.*, **73** (4),
799 1555 – 1575, <https://doi.org/10.1175/JAS-D-15-0245.1>.
- 800 Rogers, R. F., P. D. Reasor, and J. A. Zhang, 2015: Multiscale structure and evolution of hurricane
801 Earl (2010) during rapid intensification. *Mon. Wea. Rev.*, **143** (2), 536 – 562, <https://doi.org/10.1175/MWR-D-14-00175.1>.
- 803 Schechter, D. A., and K. Menelaou, 2020: Development of a misaligned tropical cyclone. *J. Atmos.*
804 *Sci.*, **77** (1), 79 – 111, <https://doi.org/10.1175/JAS-D-19-0074.1>.
- 805 Schechter, D. A., and M. T. Montgomery, 2003: On the symmetrization rate of an intense geophysical
806 vortex. *Dyn. Atmos. Oceans*, **37** (1), 55–88, [https://doi.org/10.1016/S0377-0265\(03\)00015-0](https://doi.org/10.1016/S0377-0265(03)00015-0).

- 807 Skamarock, W. C., and Coauthors, 2008: A description of the advanced research WRF
808 Version 3. Tech. rep., University Corporation for Atmospheric Research. <https://doi.org/10.5065/D68S4MVH>.
- 810 Tang, B., and K. Emanuel, 2012: Sensitivity of tropical cyclone intensity to ventilation in an
811 axisymmetric model. *J. Atmos. Sci.*, **69** (8), 2394–2413, <https://doi.org/10.1175/JAS-D-11-0232.1>.
- 813 Tang, B. H., and Coauthors, 2020: Recent advances in research on tropical cyclogenesis. *Trop.
814 cyclone res. rev.*, **9** (2), 87–105, <https://doi.org/10.1016/j.tcr.2020.04.004>, URL <https://www.sciencedirect.com/science/article/pii/S2225603220300187>.
- 816 Tao, D., 2015: Dynamics and predictability of tropical cyclones under vertical wind shear. Ph.D.
817 thesis, The Pennsylvania State University.
- 818 Tao, D., and F. Zhang, 2014: Effect of environmental shear, sea-surface temperature, and am-
819 bient moisture on the formation and predictability of tropical cyclones: An ensemble-mean
820 perspective. *J. Adv. Model. Earth Syst.*, **6**, 384–404.
- 821 Tao, D., and F. Zhang, 2015: Effects of vertical wind shear on the predictability of tropical cyclones:
822 Practical versus intrinsic limit. *J. Adv. Model. Earth Syst.*, **7**, 1534–1553.
- 823 Wang, Z., 2012: Thermodynamic aspects of tropical cyclone formation. *J. Atmos. Sci.*, **69** (8),
824 2433–2451, <https://doi.org/10.1175/JAS-D-11-0298.1>.
- 825 Wang, Z., M. T. Montgomery, and C. Fritz, 2012: A first look at the structure of the wave
826 pouch during the 2009 PREDICT–GRIP dry runs over the Atlantic. *Mon. Wea. Rev.*, **140** (4),
827 1144–1163, <https://doi.org/10.1175/MWR-D-10-05063.1>.
- 828 WMO, 2017: Global guide to tropical cyclone forecasting. World Meteorological Organization,
829 Geneva, Switzerland, 384–396.
- 830 Zhang, F., and D. Tao, 2013: Effects of vertical wind shear on the predictability of tropical cyclones.
831 *J. Atmos. Sci.*, **70**, 975–983.